Quaternary Science Reviews 201 (2018) 261–279

Contents lists available at ScienceDirect

Quaternary Science Reviews

journal homepage: www.elsevier.com/locate/quascirev

Response of lake-catchment processes to Holocene climate variability: Evidences from the NE Tibetan Plateau

Dada Yan [a, b], Bernd Wünnemann [a, b, c, *], Yongzhan Zhang [c, **], Hao Long [d], Georg Stauch [e], Qianli Sun [a], Guangchao Cao [f]

[a] State Key Laboratory of Estuarine and Coastal Research, East China Normal University, 3663 Zhongshan North Road, Shanghai, 200062, China
[b] Institute of Geographical Sciences, Freie Universität Berlin, Malteserstr. 74-100, 12249, Berlin, Germany
[c] School of Geographic and Oceanographic Sciences, Nanjing University, Xianlin Ave. 163, Nanjing, 210023, China
[d] State Key Laboratory of Lake Science and Environment, Nanjing Institute of Geography and Limnology, Chinese Academy of Sciences (NIGLAS), Beijing East Rd. 73, Nanjing, 210008, China
[e] Department of Geography, RWTH Aachen University, Templergraben 55, 52056, Aachen, Germany
[f] Qinghai Province Key Laboratory of Physical Geography and Environmental Process, Qinghai Normal University, Wusi West Rd. 38, Xining, 810008, China

ARTICLE INFO

Article history:
Received 19 June 2018
Received in revised form
8 September 2018
Accepted 12 October 2018
Available online 26 October 2018

Keywords:
China
Paleoclimatology
Paleogeography
Sedimentology
Micropaleontology
Monsoon

ABSTRACT

Investigating the so-called Third Pole Environment (TPE) became a major concern during the last decades since it was recognized that the high-altitude region of the Tibetan Plateau (TP) is a key area for the understanding of cause-effect mechanisms driven by climate change and geodynamic processes. Studies on the hydro-climatic evolution during the Late Quaternary were mainly carried out by single lake records or alternatively by individual terrestrial sites. Integrated source-to sink studies considering lake–catchment interactions were extremely seldom utilized. We investigated such relationships in the Kuhai Basin on the north-eastern Tibetan Plateau and analysed sedimentary processes based on 30 onshore sections and three sediment cores from different locations and water depth in the lake basin. Grain size variations, ostracod assemblages, geochemical proxies and absolute dating (luminescence, radiocarbon, $^{210}Pb/^{137}Cs$) were applied as key indicators that reveal interacting sediment fluxes under different hydro-climatic settings during the Younger Dryas interval and the Holocene. Our results indicate that wind-induced transportation processes and allocation of respective aeolian sands in the catchment are attributed to distinct phases of reduced effective moisture availability during summer time. Those phases corresponded to weak summer monsoon influence during the Younger Dryas interval, the Early Holocene (11.6–7.5 ka), dry-cold interlude (DCI: ca. 4.5–3.0 ka), Dark Ages Cold Period (DACP: ca. 1.8–1.1 ka) and the Little Ice Age (LIA: ca. 0.6–0.1 ka). Contemporaneous low lake levels during these periods corresponded with respective aeolian sand flux and variable composition of mixed sediments (fluvial and aeolian) in lake deposits. Different flux rates at the core sites could be assigned to local conditions in respect to inflow behaviour of individual drainage systems and nearshore morphology. Aeolian deposits in the catchment were not always preserved and underwent re-mobilisation during succeeding episodes and/or erosion during phases of high water availability. Wetter climatic conditions during the Mid-Holocene (ca. 7.5–5.1 ka), Roman Warm Period (RWP: ca. 2.8–1.5 ka) and Medieval Climate Anomaly (MCA: ca. 0.9–0.6 ka) revealed significant lake level rise due to enhanced river discharge, well documented by highest suspended flux rates, disappearance of ostracod communities at core sites and very low sand input. Climate shifts during the Holocene were linked to variations in effective moisture supply under the influence of the Asian summer monsoon (ASM) and the interplay with the mid-latitude westerlies (MLW). Cold-dry phases were likely a response to North Atlantic climatic anomalies transmitted by the MLW across the TP.

© 2018 Elsevier Ltd. All rights reserved.

* Corresponding author. State Key Laboratory of Estuarine and Coastal Research, East China Normal University, North Zhongzhan Road 3663, Shanghai 200062, China.
** Corresponding author. School of Geographic and Oceanographic Sciences, Nanjing University, Xianlin Ave. 163, Nanjing 210023, China.
E-mail addresses: wuenne@zedat.fu-berlin.de (B. Wünnemann), zhangyzh@nju.edu.cn (Y. Zhang).

https://doi.org/10.1016/j.quascirev.2018.10.017
0277-3791/© 2018 Elsevier Ltd. All rights reserved.

1. Introduction

Reconstructing climate variability over the Tibetan Plateau (TP) has been a major concern during the last decades. There is wide agreement among scientists that the interplay between the Asian monsoon systems and the mid-latitude westerlies are important drivers during the last glacial-interglacial cycles controlled by orbital-scale changes in insolation, ice volume and sea level changes (Colman et al., 2007; An, 2000, 2012; Cheng et al., 2016). The spatio-temporal influence of the Asian summer monsoon in high altitude regions of the TP and its response to environmental changes during the Late Quaternary however, is still a matter of debate (e.g., An, 2000, 2012; Boos and Kuang, 2010; Yao et al., 2013; Zhang et al., 2011; Liu et al., 2015a; Ramisch et al., 2016; Hou et al., 2016, 2017). Commonly multi proxy studies on single records from lakes (e.g., Wu et al., 2006; Mischke et al., 2008, 2010; Mischke and Zhang, 2010; Opitz et al., 2012; Qiang et al., 2017) or alternatively from terrestrial sites (Yu and Lai, 2012; Stauch et al., 2012; IJmker et al., 2012; Liu et al., 2015b; Qiang et al., 2014, 2016; Hu et al., 2018) were frequently used to infer large-scale shifts in the climatic system in respect to hydrodynamic variations or aeolian flux. The majority of published records from the Tibetan Plateau and adjacent regions are based on proxy data derived from sediment parameters (e.g. grain size, sediment geochemistry, fossil remains, biomarkers) retrieved from a lake, independent from lake size and catchment characteristics (e.g., Wu et al., 2006; Liu et al., 2007; Mischke et al., 2008, 2010; Zhang and Mischke, 2009; Henderson et al., 2010; An et al., 2012; Hou et al., 2012, 2017; Chen et al., 2015; Rao et al., 2016; Qiang et al., 2017; Hu et al., 2018). Such proxy records yielded different results due to conflicting data interpretation of individual proxies (e.g., Holmes et al., 2009; Chen et al., 2016), chronological uncertainties (e.g., Mischke et al., 2013; Hou et al., 2012) and resulting paleoclimatic inferences. Comparison of proxy data from multiple cores of individual lake systems (Morrill et al., 2006; Opitz et al., 2012; Wünnemann et al., 2012; Yan and Wünnemann, 2014) revealed that despite local differences in sediment composition overall hydrodynamic processes and related local climatic impact were explained without full integration of catchment dynamics by hard data (e.g., Morrill et al., 2006; Wünnemann et al., 2012). Considerations of such interacting processes between a certain lake and its catchment however, were very seldom utilized, although necessary for a comprehensive understanding of underlying mechanisms that influenced environmental change of local, regional or even global significance.

The hydrologically closed Lake Kuhai and its catchment on the north-eastern TP were selected as an ideal location in the transitional region of summer monsoon influence as the basin reacted very sensitively to hydro-climatic changes during the Holocene. We demonstrate close relationships between catchment dynamics, transportation processes and lake hydrology by the comparison of sediment cores from the lake with sediments from 30 onshore sections in order to validate spatio-temporal sediment flux and the interaction between aeolian, fluvial and lacustrine processes.

2. Study site

Lake Kuhai (35.3° N; 99.2°E, Fig. 1) at 4132 m elevation is situated on the north-eastern part of the Tibetan Plateau. Catchment and lake basin are located in the marginal zone of the East Asian Summer Monsoon (EASM). Influence by the mid-latitude westerlies throughout the year is high (Yao et al., 2013; Maussion et al., 2014; Curio and Scherer, 2016). The 49.12 km^2 large saline lake is hydrologically closed (no outflow) with maximum water depth of 22.3 m. Its catchment is about 711 km^2 comprising mountain ridges of less than 5000 m elevation and wide alluvial-fluvial fans surrounding the lake basin. The highest north-south striking mountain range along the eastern border of the basin forms the watershed to the Yellow River. There is no morphological evidence of glaciated areas within the catchment, although former glaciers existed in the neighbouring catchment of Lake Donggi Cona (Rother et al., 2017). The push-up structure of the Anyemaqen Mts (Van der Woerd et al., 2002) is still glaciated but is outside the Kuhai catchment. Permafrost within the catchment is wide-spread. Eight rivers around the lake basin are only episodically active during the rainy season in summer time. Three rivers located in the eastern, south-eastern and south-western sub-catchments however, provide water the year round except during the frozen period in winter between December and March (Fig. 1). The lower parts of the catchment consist of wide-spread wetlands in the transitional zone between the lake and inclining fluvial fans toward the upper mountain slopes. Dune-covered areas exist in the north-eastern part of the lake catchment as well as on the island in the southern part of the lake and along mountain slopes on the western side of the lake basin.

The area is tectonically affected by the large-scale Kunlun Fault system (Van der Woerd et al., 2002; Fu et al., 2005), although not a part of it. Geological formations belong to Precambrian, Palaeozoic and Mesozoic (Triassic) series, mostly occurring as metamorphic rocks with locally different petrology. Limestone of Triassic age is only occasionally present. Sedimentary sequences of Quaternary age dominate the alluvial-fluvial fan generations and the lake bottom.

The lake water is saline with an electric conductivity of 19.9–22.8 mS/cm. Its pH is spatially variable and ranged between 7.2 and 8.7, measured in 2015 and 2016. Total dissolved solids (TDS) reached values of up to 20.1 g/l, which accords to a reduced transparency of only 6–7 m. The lake hosts high amounts of green algae and aquatic plants, such as *Potamogeton* sp., the latter only occurs down to a water depth of 6 m.

Climate information is based on the observation data from the nearest weather station (Maduo county, National Metrological Information Center: http://data.cma.gov.cn/data/detail/dataCode/A.0029.0004.html station code: 56033) with 30 years (1981–2010) records. The mean annual temperature and precipitation was calculated to −3.3 °C and 332.5 mm, respectively. However, the mean annual evaporation of about 1000 mm (Ling, 1999) exceeds the precipitation by three times. Approximately 56% of the annual precipitation falls during the summer season between July and September.

The modern vegetation in the Kuhai catchment area is dominated by taxa of high-alpine meadows mainly as *Kobresia pygmaea* and *Stipa purpurea* formations, with some alpine shrubs such as *Salix orithrepha*, *Saussurea* spp. and *Dasiphora* (*Potentilla*) *fructicosa*, in the southeastern catchment (Hou, 2001; Kürschner et al., 2005). The generally sparse grassland is used as pasture for yaks, sheep and goats by local residents.

3. Methods

Fieldwork was carried out during several weeks in early summer in the years 2014–2016 comprising investigations on the lake and selected onshore sites within the Kuhai catchment.

3.1. On-shore sections

Thirty sections within the Kuhai catchment area were sampled either from naturally exposed river cuts at near-shore locations and river upstream sites, mainly along the eastern side of the lake or dug by hand (Fig. 1 and Table S1). The latter ones comprise sites on the island in the southern part of the lake, on hillslopes, dunes and

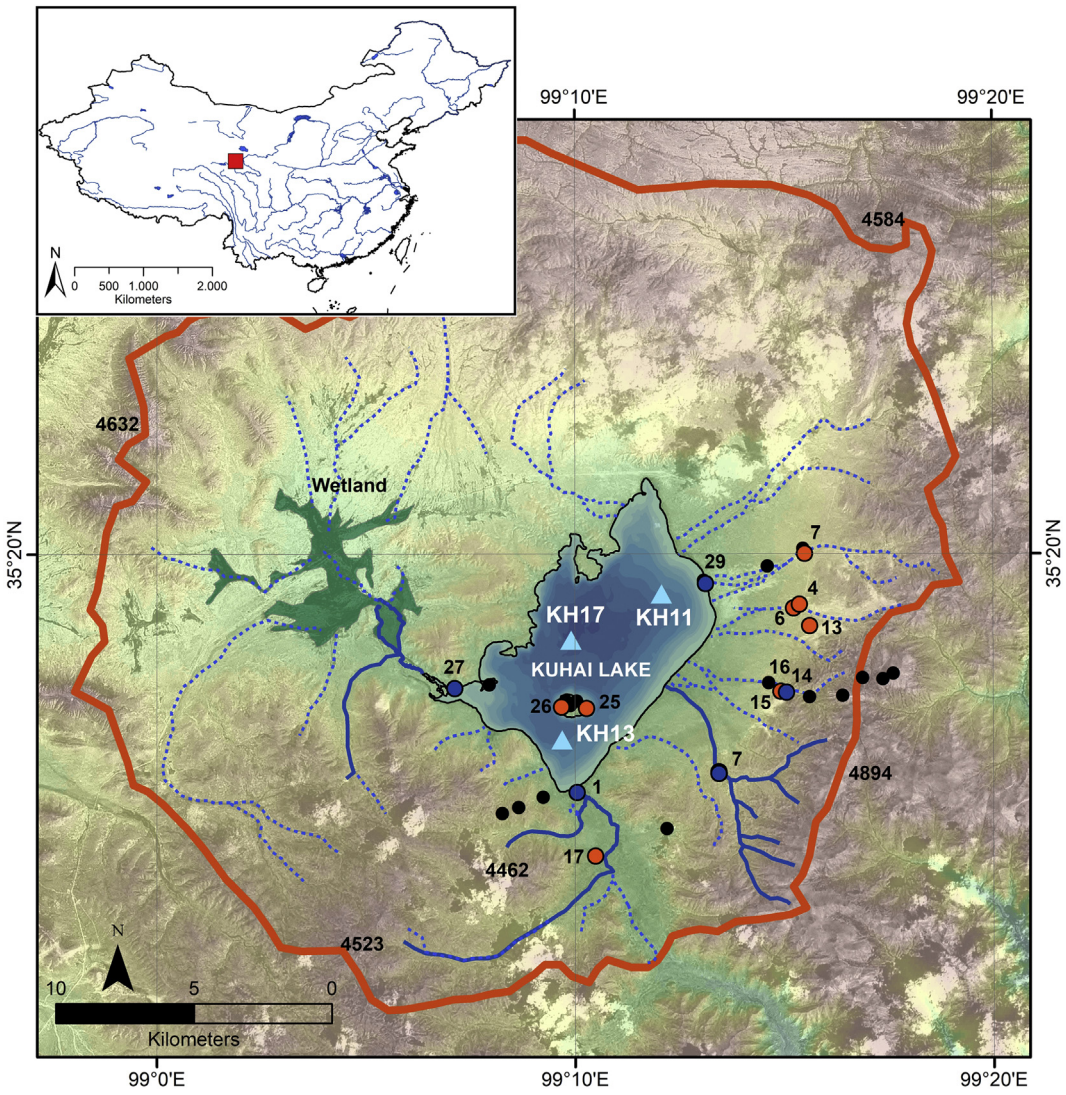

Fig. 1. Overview map of the research region. Inlet: Map of China with location of study site. Map of the Lake Kuhai with location of core sites (blue triangles) and onshore sections (red circles: lumninescence-dated sites; blue circles: AMS dated sites; black circles: sections without dating. Numbers indicate sites mentioned in the text. Dotted blue lines: episodic rivers (July–Sept.); blue lines: perennial rivers (March–December). Red line: Kuhai catchment with elevation (meter a.s.l.) of mountain peaks. (For interpretation of the references to color in this figure legend, the reader is referred to the Web version of this article.)

shoreline cuts. Sampling of the sections for further analyses followed section stratigraphy and lithology. Labelling of the sections refers to different years of sampling (KH4, KH9: 2014; all KHS sections: 2015, 2016). Here we mainly refer to dated sections.

3.2. Off-shore sediments

Lake sediments were retrieved by piston coring (UWITEC system) in PVC liners of 2 and 3 m individual length. Coring referred to 3 different locations and water depth, of which only the core in the lake's center reached 6.84 m sediment depth (Fig. 1). Additional surface sampling across the lake was applied to identify modern sediment composition and ostracod communities.

3.3. Dating (^{210}Pb/^{137}Cs, radiocarbon AMS, luminescence)

Radionuclide dating (^{210}Pb/^{137}Cs) on the upper 25 cm of sediment core KH13 in 1 cm resolution was performed at Nanjing Institute of Geography and Limnology, Chinese Academy of Science (NIGLAS). Seventeen radiocarbon ages from onshore sections were determined at Beta Analytics, Miami, USA, referred to individual terrestrial and aquatic plant remains, bulk organic matter and the alkali soluble (humic) and alkali insoluble (humin) fractions. In addition, 45 AMS ages refer to the sediment cores KH11, 13 and 17, listed in Table S2, dated at the same laboratory. Cores KH14 and KH17 were retrieved from the same site. They were individually dated and later spliced to a composite core. All calibrated age models refer to the R algorithm in Bacon (Blaauw and Christen, 2011) with reference to the Intcal13 dataset (Reimer et al., 2013).

A total of 25 samples from sections containing aeolian deposits in the Kuhai catchment were dated by luminescence method at the laboratories of NIGLAS and School of Geographic and Oceanographic Sciences, Nanjing University. Owing to low luminescence intensity of quartz in these sediments, the K-feldspar fractions were selected for dating. Sample preparation followed the methods provided by Long et al. (2014). For more details refer to the supplement and Table S2.

3.4. Grain size analyses

Grain size analysis was performed on samples from sections and sediment cores following the procedures according to ISO Norm 14688−1, 2011 and Yan and Wünnemann (2014). Grain size distributions between 0.02 and 2000 μm were determined, using a Malvern Mastersizer 2000 Analyzer at Nanjing University, China.

3.5. Endmember modelling analysis

Original grainsize data (KH11:95 samples; KH13:108 samples; KH17:610 samples) were applied for endmember modelling analysis (EMMA, Fig. 8), following Weltje (1997) and Dietze et al. (2012). The EMMA of sediment cores was based on different granulometric classes (70 for KH11; 54 for KH13; 59 for KH17), with a variable-to-sample ratio of ca. 1/1, 1/2 and 1/10, respectively. Dietze et al. (2012) mentioned that single grain-size parameters (e.g., contents of sand, silt, and clay fractions), or the associated methods of moments (e.g., mean, skewness, kurtosis; Folk and Ward, 1957) are biased when applying to multi-modal distributions. Instead, endmember modelling as a multivariate statistical method, coupled with principal component and factor analyses, allows simultaneous interpretation of all variables within the dataset for each sample (IJmker et al., 2012) in terms of sediment transport processes and the identification of depositional environments (Dietze et al., 2013; Wang et al., 2015; Yan, 2017; Yan et al., 2017).

3.6. Geochemical analyses

Geochemical components organic matter (OM) and total carbonates (CO_3) in sediments from sections were used to estimate organic compounds and carbonates in lacustrine, fluvial and aeolian sediments. They were measured by loss on ignition (LOI) at Nanjing University, following the procedures described by (Heiri et al., 2001). Due to grain size effects we corrected the data against fractions <63 μm, implying that OM and carbonate was mainly concentrated within fine fractions. Measured results were attached to section profiles (see supplementary information) and carbonates to the cores (Fig. 9 and Fig. S11).

3.7. Ostracod analyses

For the identification of ostracods in selected samples ca. 3 g of dry bulk sediment from 53 section samples and 1005 samples from the three lake cores were treated according to Frenzel et al. (2010), using ca. 5% H_2O_2. Dispersed samples were wet-sieved using 125 μm and 250 μm meshes. Ostracod species identification and counting under a stereoscopic microscope was performed with reference to Meisch (2000), Griffiths and Holmes (2000) and Yan and Wünnemann (2014).

4. Results

4.1. Chronology − radiocarbon dating

Lake sediments in cores KH11, KH13 and KH17 dated by radiocarbon from different fractions (aquatic plant remains, bulk organic matter, insoluble and soluble fractions) resulted in individual age models (Fig. 2, Table S2). In addition, radionuclide dating by $^{210}Pb/^{137}Cs$ for the upper 24 cm of core KH13 was used to define zero BP (1950 AD), which occurred at 10 cm sediment depth. Linear regression between individual ages and 10 cm sediment depth in all cores revealed considerable reservoir errors (RE), which are very common in lakes of the Tibetan Plateau and thus subject to various discussions (Zhang et al., 2006; Wu et al., 2009; Hou et al., 2012; Wünnemann et al., 2012; Mischke et al., 2013). Commonly, the influence of dead/old carbon derived from limestones in the catchment (Lockot et al., 2015) is of minor importance for the Kuhai records as carbonate rock in the catchment is rare. We assume that the majority of older carbon contribution influencing the RE at different locations in the lake is derived from other sources in the catchment.

Parallel dating of selected samples revealed age differences between 100 and 1500 years (mean 500 years). Hence, we used grain size results to decide which of the ages would better fit to a regression between ages, given the assumption that coarser sediments indicate faster sediment accumulation rates (SAR). In single cases we used mean values between given ages, once the age differences between the dated fractions were small (Table S2).

We avoided linear regression through the entire record (e.g., An et al., 2012), because a constant SAR could not be expected. As a result, all sediment cores revealed different mean REs of 2041, 2495 and 2550 years for cores KH11, KH17 and KH 13, respectively, taking into account that RE likely varied through time (Table S2). As individual REs in lake records are still hardly detectable and RE-free terrestrial organic material was not found we used a mean RE, leading to a general age uncertainty of ca. 100−150 years in the respective records. Ages too far away from individual regression lines were considered as outliers and thus discarded from the age models (Fig. 2). Sediments from core KH17 traced back to 13.6 cal ka BP, while cores KH11 and KH13 only covered the last roughly 4.0 cal ka BP.

AMS ages from off-shore sections were dated on terrestrial plants, soil organic matter (KHS1, KH9, KHS14) or fluvio-lacustrine deposits (KHS1, KHS27, KHS29, Fig. 3, Table S2). Lacustrine deposits found in sections, were also subject to certain RE. This error however, could not be defined and might have been different from deposits in the lake. Hence, the respective ages may indicate maximum ages of deposition.

4.2. Chronology - luminescence dating

Twenty-five luminescence ages from eight sections in the Kuhai Lake catchment were determined on K-feldspar (Table S3, Fig. 3). The dune sand in section KH4 however provided ages derived from both quartz and K-feldspar minerals. They show deviations of 70−170 years for ages <1.0 ka and 1430 years in the lower part of the section (4.38 ka/2.95 ka, Fig. S3). For dose rate calculation, the contractions of nuclides (U, Th, and K) were measured by both inductively coupled plasma mass spectrometry (ICP-MS) and neutron activation analysis (NAA) methods. The ages from section KH4 were calculated from NAA data only. Both sets of dates derived from ICP and NAA show small differences within errors. In order to compare the timing of wind-blown sediment deposition of all dated sections, NAA-based ages from K-feldspar were used for discussion including the younger quartz-age from section KH4.

Most of the luminescence ages were obtained from sandy aeolian deposits, including sandy loess. Only two ages refer to loess deposits in section KHS17 (Fig. S6) which range between 4.5 ka ± 0.63 and to 9.2 ± 0.57 ka (Tab. S3). The section KHS 15, which contained sandy loess, was dated to 0.52 ± 0.05 ka, 0.41 ± 0.03 ka and 1.81 ± 0.17 ka. All other sections contained pure aeolian sand and showed two different time phases of deposition: during the early Holocene (8−11 ka), dated in sections KHS 25 and KHS 26, and during the late Holocene (0.2−4 ka) based on data from sections KHS 6, KHS 7, KHS13 and KH 4 (Figs. S2-S8).

4.3. Aeolian deposits in sections

Most of the investigated sections in the Kuhai catchment

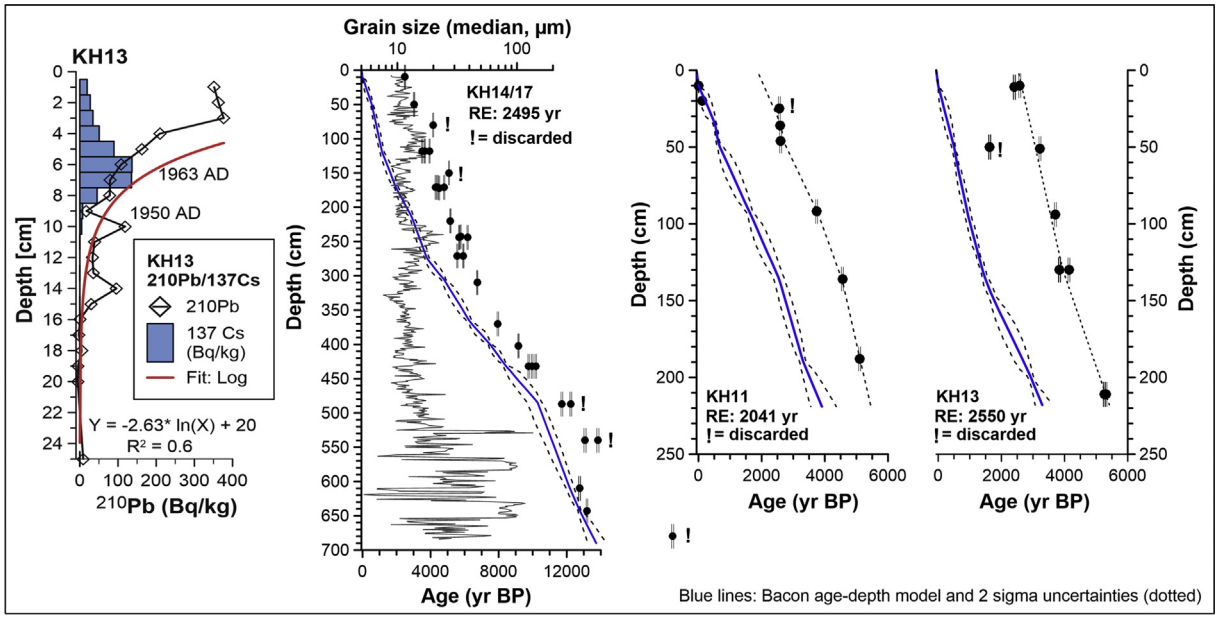

Fig. 2. Age models for cores KH11, KH13 and KH14/17; $^{210}Pb/^{137}Cs$ radionuclide dating results for the upper 25 cm of core KH13. Black dots with error bar are the original AMS ages from different organic fractions (Table S2). The blue lines denote the Bacon age model with 95% confidence levels (dotted lines). (For interpretation of the references to color in this figure legend, the reader is referred to the Web version of this article.)

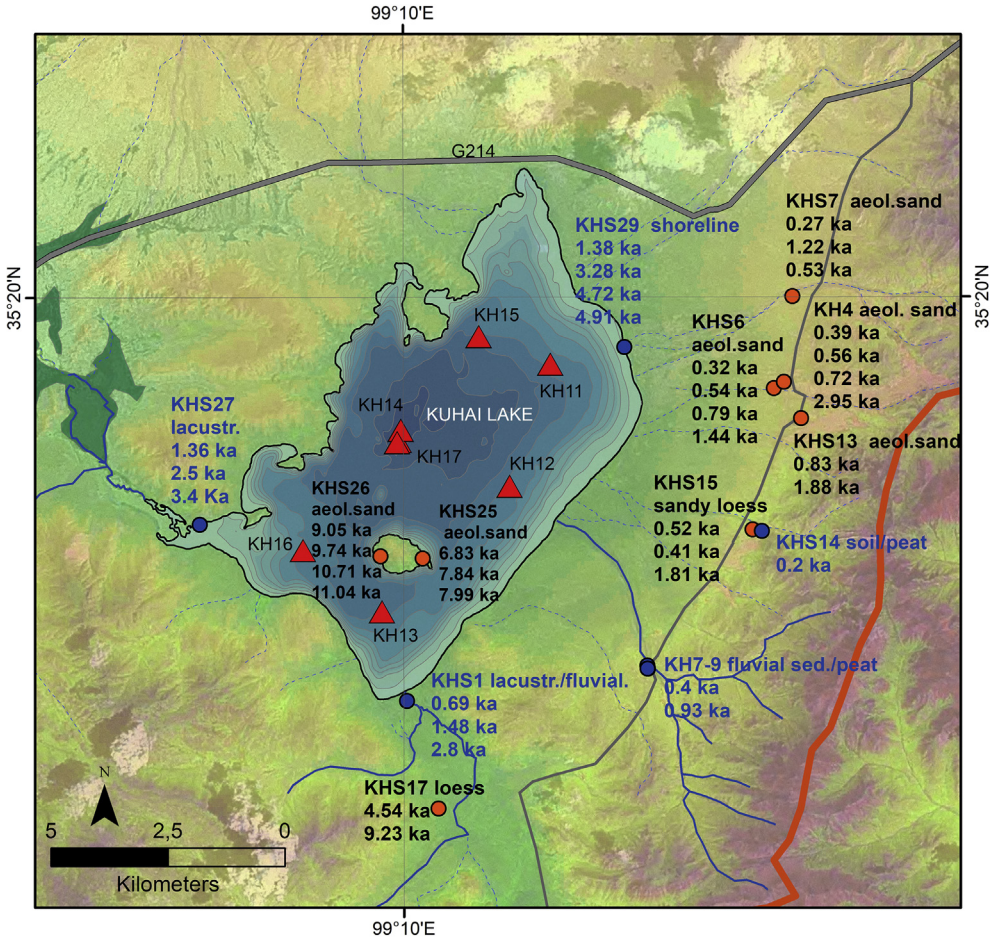

Fig. 3. Overview map of dated onshore sites in Lake Kuhai catchment.

provided sediment sequences of aeolian origin above the permafrost table, bedrock or fluvio-alluvial sequences. The section KHS26 located at the western slope of the rocky island (Fig. 3) ca. 15 m above the modern lake level provided >3 m thick aeolian sand dated to between 11.04 ka and 9.05 ka (Fig. 4A). Unimodal grain size distribution curves (main modes at 120–180 μm) are characteristic for dune sand in this region. Finer components (silt: mode <10 μm) interbedded as silt-lenses in sand fractions occurred in the lower part of the section. Section KHS25 on the island further NE (Fig. S8) showed a fining-up succession from aeolian fine sand to sandy loess and loess (115-50 cm depth), overlain by sandy loess in which the modern brown soil developed. Lumninescence ages indicate deposition of sand and sandy loess between 8.0 ka and 6.83 ka. Loess and sandy loess are younger but of unknown age.

Section KHS15 ca. 115 m above the modern lake in the eastern sub-catchment provided ca. 200 cm thick well-sorted aeolian coarse silt to fine sand which was luminescence-dated to between 1.81 ka (165 cm depth) and 0.52 ka (75 cm depth, Fig. 4B). Two paleosol layers enriched in organic matter below the modern brown soil occurred at 25–40 cm depth and 90–105 cm depth. Samples from all parts of the section revealed uni-modal grain size composition mainly in the fine sand (~60–180 μm) and few in the coarse silt fraction (~40–60 μm). Top and bottom sands were slightly coarser (>200 μm).

In section KHS14 a paleosol similar to that one in KHS15 was dated to 193 ± 27 cal. yr BP. Other sections along the eastern alluvial fans (KHS6, KHS7) and in semi-fixed dunes (KH4, KHS13) provided similar successions mainly composed of aeolian fine sand free of paleosols (Figs. S2-S5). They date to between 2.95 and 0.24 ka indicating quite young ages of last deposition.

4.4. Fluvial deposits in river terraces (KH9)

Two distinct terrace systems developed at the eastern side of the lake as a result of sequential incision of the rivers into the alluvial/fluvial fans. The higher one, (T1 in Fig. 5), ca. 12–16 m above the modern river bed, consisted of coarse fluvial gravels, mainly with angular shape, indicating short-distance transport with coarsening-up towards the upper catchment. Lithology of the material confirms local provenance mainly composed of metamorphic rocks of Permian age and to a lesser extent, Triassic components (sandstone, limestone). The latter components were only observed in the terrace systems of this river, while all others provided Permian and Proterozoic facies, in agreement with the geological map (Fu et al., 2005).

The lower terrace (T2, Fig. 5), 1.2 m in height also consisted of mainly angular-shaped coarse gravels of local provenance, interrupted by organic-rich fine material with plenty of terrestrial plant remains (peaty wetland facies). The age points to deposition during the Little Ice Age (403 ± 44 cal. yr BP). An even older age was

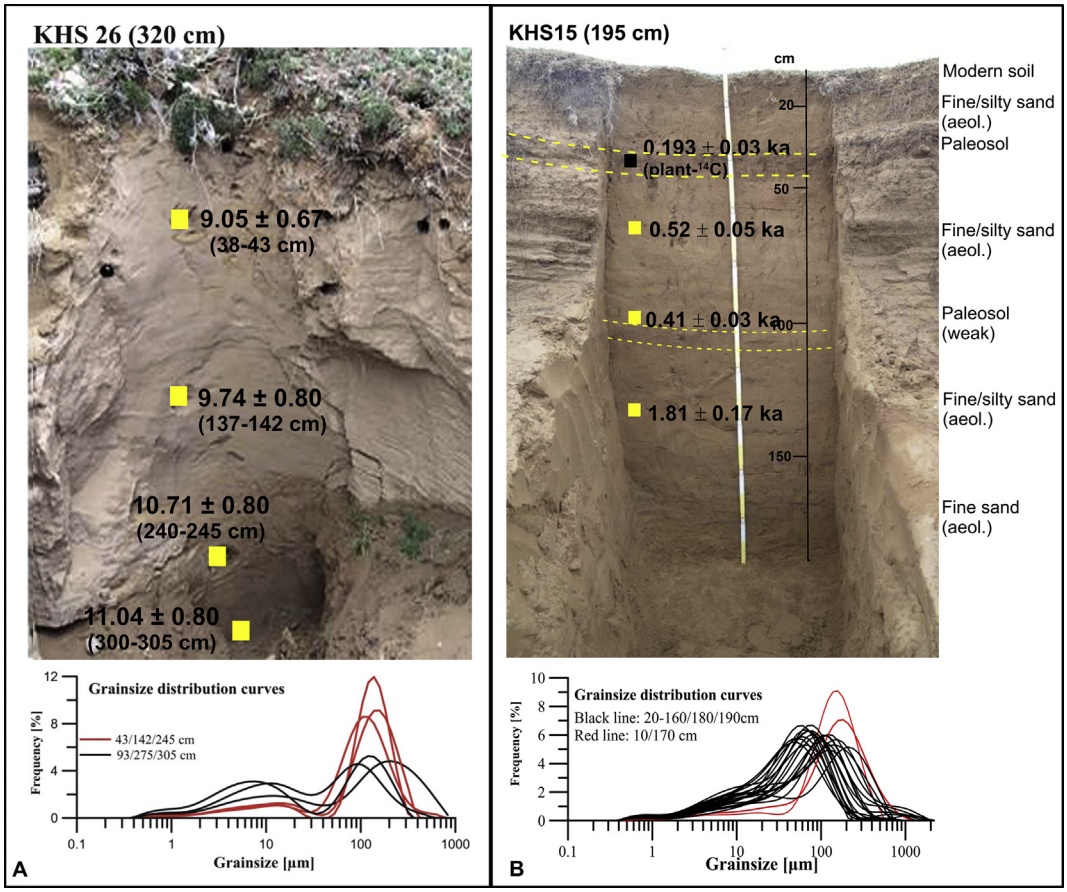

Fig. 4. A: Photo of section KHS26 at the south-western flank of the island (southern part of Lake Kuhai). More than 3 m thick aeolian sands were deposited during the early Holocene. Position and lumninescence ages are marked in the photo. Grain size composition (lower panel) indicates generally fine to medium sand fractions (red lines, partly mixed with finer components in the lower part of the section (black lines). **B:** Section KHS15 uphill aeolian sand section with lumninescence ages and (paleo) soil layers. Grain size compositions (lower right) indicate sandy loess to fine sand. For locations see Fig. 3. (For interpretation of the references to color in this figure legend, the reader is referred to the Web version of this article.)

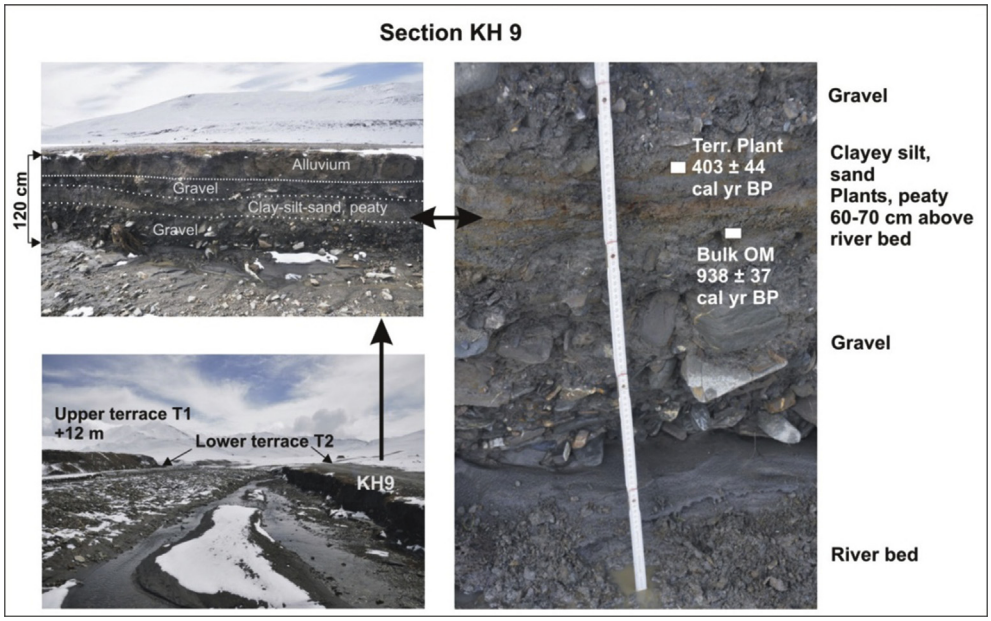

Fig. 5. Section KH9, lower terrace T2, river bank of the main river in the eastern catchment. Upper left: T2 with distinguishable lithofacies; lower left, overview of the terraces T1 and T2, view to east; right side: detail of section KH9.

obtained slightly below (938 ± 37 cal. yr BP) on bulk organic matter.

4.5. Fluvio-lacustrine deposits in nearshore sections

Two onshore sections (KHS1, KHS29: for location see Figs. 1 and 6) close to inflowing river beds near the modern shoreline of Lake Kuhai showed alternating fluvio-lacustrine and fluvial successions of sandy to silty sequences. In section KHS1 (Fig. 6A) alternating silt and sand layers were interrupted by a distinct gravel layer at 90–130 cm depth. Grain size composition mainly occurred as bi-modal curves with modes between ~40 μm and 100 μm (6–35 cm depth) and 25–180 μm (40–70 cm depth). Permafrost occurred at ca. 80 cm depth. The sequences below (70–156 cm depth) displayed mixed sediment composition with modes between ca. 15 μm and 180 μm. Fine-clastic sediments contained the ostracod species *L. inopinata* and *Ilyocypris* sp. Sediments between 80 and 160 cm depth were dated to between 0.69 cal ka BP and 2.8 cal ka BP.

In section KHS29 (Fig. 6B) variations between silt and sand layers with variable modes at 6 μm, 20–40 μm and 100->300 μm and coarse gravelly sediments at the top part (170–220 cm height) were characteristic compositions in this section. A distinct 2–4 cm thick layer of aquatic plant fragments (seagrass) occurred at 178–182 cm height, interbedded in coarse sand to gravelly sediments. Ostracods (generally low amounts) were found in several layers, identified as *L. inopinata* and *Ilyocypris* sp.

The section KHS27 in a cliff-like position of an island in the south-western part of the modern lake (1.5 m above the modern waterline) was AMS-dated to 3.4 and 1.36 cal ka BP. The sediments were mainly composed of organic-rich clayey silt with intercalated sandy layers (Fig. S9), assigned to semi-lacustrine deposits. Sediments were horizontally bedded although other parts of the cliff section showed cryoturbation features. Frozen sediments at the bottom (equal with the modern water level) indicate the presence of permafrost. Ostracods in this section comprised *L. inopinata* as the dominant species. *F. rawsoni* and *Ilyocypris* sp. occurred in the lower part (40–60 cm height) and frequently in the top part (95–130 cm). *E. mareotica* was only found in one sample close to the bottom of the section (40 cm height) together with all other species.

4.6. Morphological context of lake sediment cores

Sediment core KH11 (35.32°N, 99.20° E) was retrieved from 13.26 m water depth (Fig. 1). The site is connected with the fluvial-alluvial fan on the north-eastern side of the lake basin. Inflowing rivers passing flat wetlands are only episodically active during the summer season (3–4 months). Transported coarser sediments from the catchment along the pathways to the main lake body are currently filtered in the wetlands and by the dense plant cover in the littoral zone. As a result, fine suspended load is the major component deposited in the lake, notably in the lake center.

Sediment core KH13 (35.27°N, 99.16°E, 13.7 m water depth) was obtained from a near-shore location in the south-east of Lake Kuhai in a small sub-basin between the lake shore and the island (Fig. 1). This site is located in close proximity to the river valley bounded by two terrace systems as mentioned before (see Fig. 5). A larger, slightly inclining wetland (floodplain) once connected with the lake is now separated by a 2 m high shoreline, locally cut by a meandering river, which is active throughout the year, except for the frozen period. Hence, sediment supply to the lake basin occurs during 8 months of the year, depending on seasonally variable inflow behaviour.

Core KH17 (35.31°N, 99.17°E) was retrieved from the deepest part of the main basin at 20.6 m water depth (Fig. 1). Respective sediments reflect depositional conditions in larger distance from multiple input sources. Hence, those sediments commonly provide mixed signals derived from catchment processes, lake-internal dynamics and atmospheric conditions as a mean of individual processes.

4.7. Grain size composition and EMMA results in lake sediments (cores KH11, KH13 and KH17)

Grain size composition of three sediment cores from the lake (Fig. 7), covering the last ca. 4 ka (KH11, KH13) and 13.6 ka (KH17) displayed different distribution curves through space and time. Grain size patterns in core KH11 in relative proximity to shallow

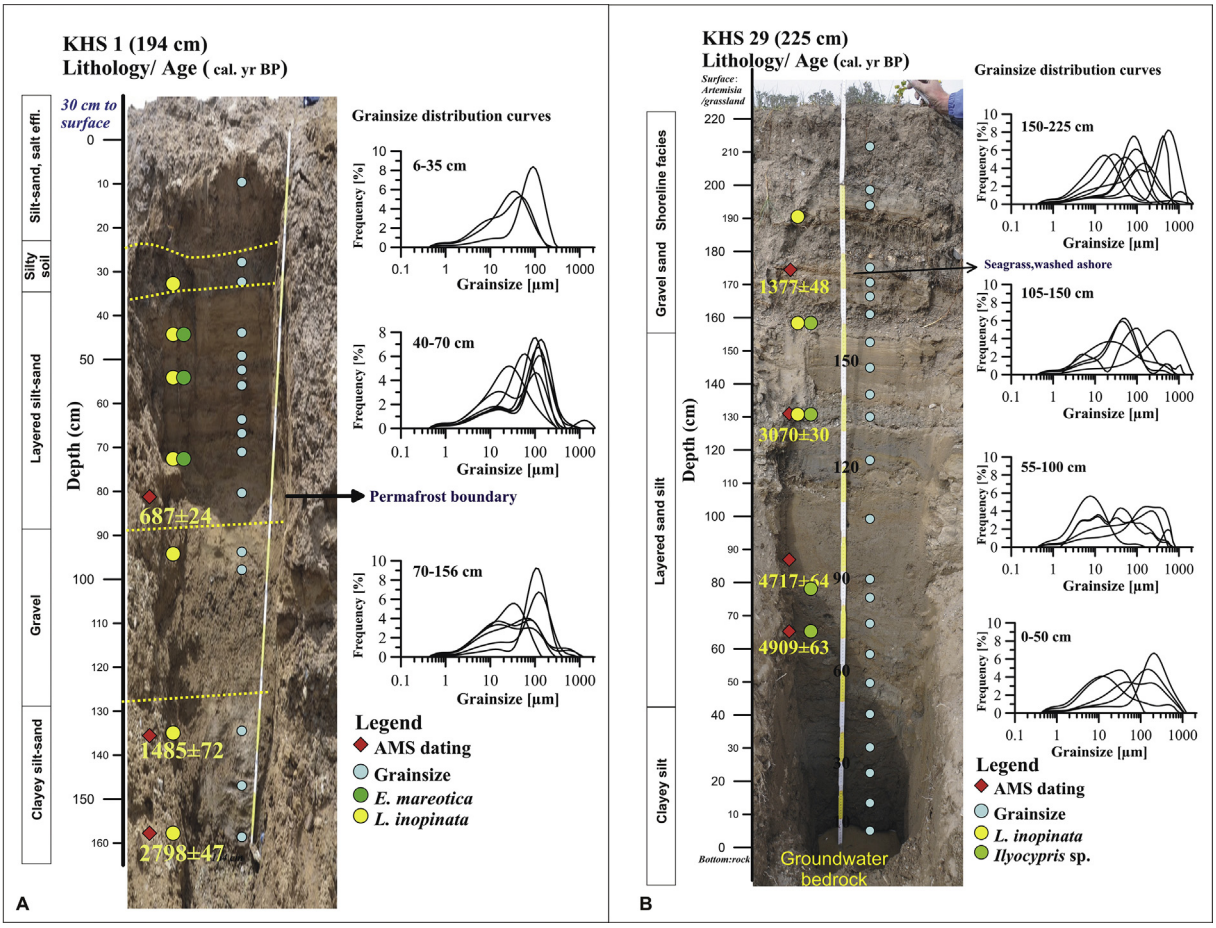

Fig. 6. **(A)** Photo of section KHS1 at the south-eastern lake side ca. 1 m above the present lake with location of samples, recorded ostracod occurrences, AMS ages and grain size curves. The permafrost boundary was detected at 80 cm depth. **(B)** Photo of section KHS29 at the north-eastern lake margin (former shoreline), ca 2.5 m above the present lake level with locations of samples, ostracod occurrences, AMS ages and grain size distribution curves for different parts of the section. For location see Fig. 3.

wetlands through-flown by episodic rivers in the north-eastern part of the lake always showed homogenous mainly unimodal grain size distribution through time within three distinguishable mean modes: 11–15 μm and 26 μm. Sand fractions remained below 15%.

Sediments in core KH13 close to the inflow region of the south-eastern river (in short distance to section KHS1) were similar to the record of KH11 (mean modes 12–15 μm) but most of them showed right-tailed shoulders (bi-modal) towards coarser components (30–35 μm). A second group of sediments with multi-modal character displayed medium-coarse silt to sand fractions with modes at 40–65 μm and 220 μm. Sediment core KH17 in the lake center provided at least 4 different types of sediment composition with modes at 12–15 μm, 30 μm, 65–70 μm and 100–160 μm, indicating higher variability of transportation processes through time (Fig. 7 and Fig. S10). Most of the samples with coarse grain size composition occurred in the lower part of the sediment record, equal to a time period between ca. 13.6 and 8.0 cal ka BP.

Sediments of aeolian origin in the Kuhai catchment and adjacent regions could be divided by mean grain size curves into loess, sandy loess and sand/dune sand, according to Stauch et al. (2012) and Yan (2017). The majority of the lake sediments are significantly finer than the mean modal values of loess deposits.

Endmember modelling analysis from all cores revealed three different bi-or tri-modal endmember curves (EMs), explaining 98% (KH11), 97% (KH13) and 97.5% (KH17) of variance (Fig. 8).

EM1 in all cores showed main modal values in the medium silt fractions (6–12 μm) and second modal values in the sand fraction (70–200 μm). Main modal values of EM2 (EM3 in KH11) occurred in the fine sand fractions (63–95 μm) with stepped right tails towards the coarser sand fractions. Minor mean modal values covered the fractions 4–6 μm. The main modal value in EM3 (EM2 in KH11) covered the medium silt fraction (20–25 μm), while minor modal values occurred in the sand fractions (70->200 μm), similar to EM1. For core KH17 see also Fig. S10.

4.8. Carbonate content in sediment cores

Total carbonate (CO_3) in sediment core KH17 varied between 1.3 and 45.8% (Fig. 9B). Continuously low values occurred at 14.5–11.5 and 2.8–0 cal ka BP. Fluctuating and highest values were recorded between 11.0 and 7.9 cal ka BP and at 4.7–3.0 cal ka BP. Intermediate but slightly declining values occurred at 7.5–5.2 cal ka BP. Carbonates in cores KH11 and KH13 varied between 4.4 and 20.2% (KH11) and between 4.1 and 33% (KH13), respectively, roughly resembling the trends in core KH17 although varying with larger amplitudes (Fig. S11).

4.9. Ostracod distribution in lacustrine deposits

Five ostracod species were identified in onshore sections) and nearby small ponds, identified as *Eucypris mareotica* (Fischer, 1855),

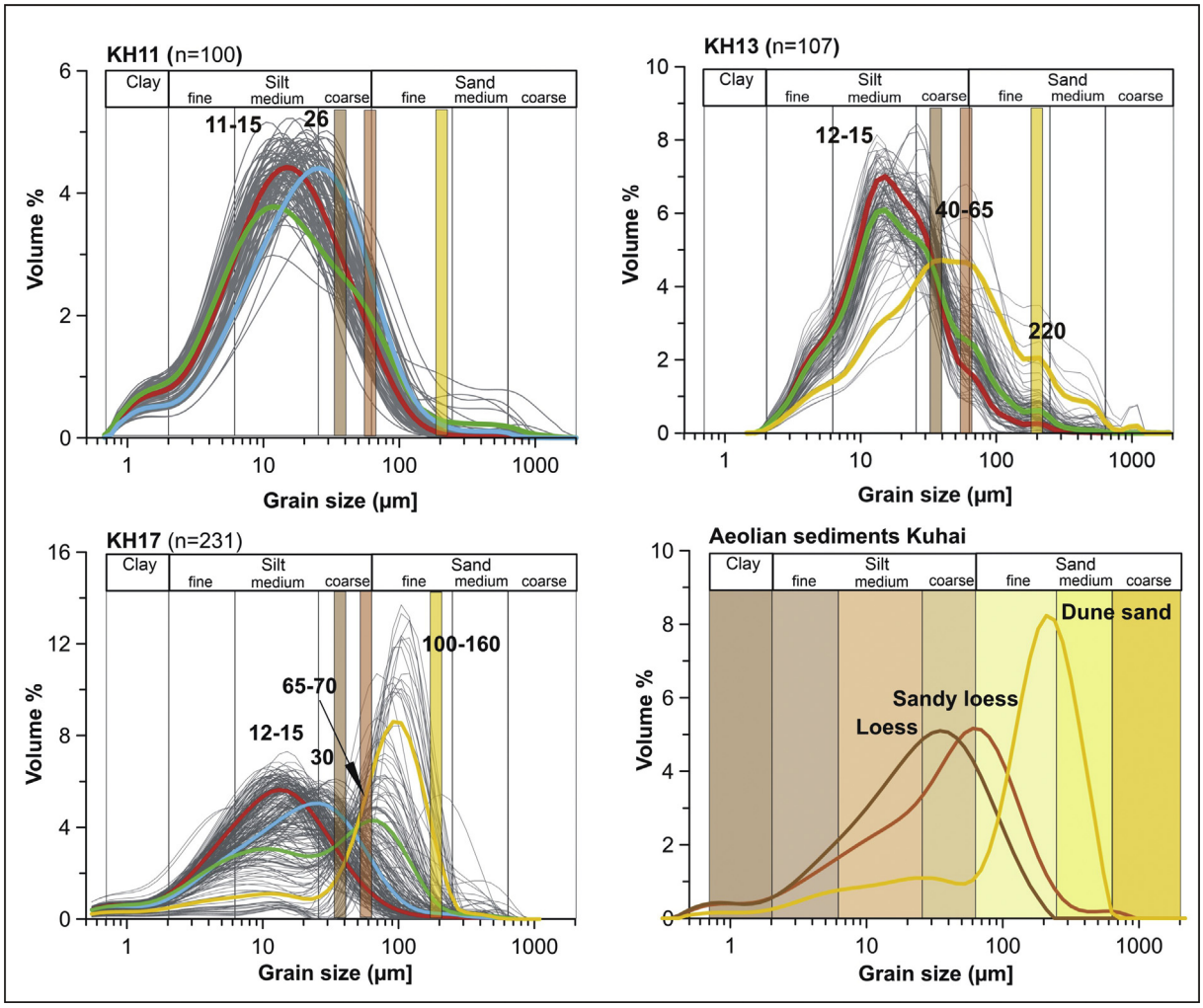

Fig. 7. Grain size distribution curves of sediments from cores KH11, KH13 and KH17 with mean values (colored lines) for different modal values in comparison with aeolian sediments (lower right panel). Marked colored bars in the core records indicate the modal ranges for loess, sandy loess and dune sand. Numbers indicate peak (modal) values.

Limnocythere inopinata (Baird, 1843), *Ilyocypris* spec., *Fabaeformiscandona rawsoni* (Tressler, 1957) and *Tonnacypris edlundi* (Van der Meeren et al., 2009). They only occurred irregularly in sections with semi-lacustrine sequences (Figs. 4 and 6). In lake surface sediments however, only the two species *E. mareotica* and *L. inopinata* were found (Fig. S10A) and were recorded from few sites in relatively shallow water above 12 m water depth in different amounts. In sediment cores ostracods occurred in relatively high abundances between 4.0 and 2.8 cal ka BP and after roughly 1.5 cal ka BP (Fig. S10B), but they did not occur in the upper 15 cm of the cores (the last ca. 100 years). High abundances in core KH17 were also recorded for the time interval between 11.7 and 7.7 cal ka BP with short interruptions centering at 11.2, 8.4 and 8.1–7.8 cal ka BP. Low abundances or absence of ostracods between 2.8 and 1.8 cal ka BP are recorded in all cores. In core KH17 absence of all species also refers to the period 8.0–5.1 cal ka BP (Fig. 9 and Fig. S10B).

5. Discussion

A number of onshore sections in the Kuhai catchment and the spatio-temporal distribution pattern of lake deposits from three sediment cores were investigated for a better understanding of interactions between on- and offshore processes. Those processes are closely tied with the topographic and geomorphological settings of the catchment (Wünnemann et al., 2015). The topography of km-wide alluvial fans and wetlands in the northern, north-western and eastern sub-catchments hosting the majority of drainages in comparison to steeper mountain slopes close to the lake basin along the southern and western sub-catchments are important characteristics for the interpretation of spatially diverse sediment fluxes (IJmker et al., 2012; Stauch et al., 2012, 2014). Two major processes within the catchment and lake basin refer to aeolian transport/deposition and fluvial activity. Most of the onshore sections revealed aeolian deposits (sand, sandy loess and loess) of different age, whilst three sections were composed of pure fluvial (KH9) and fluvio-lacustrine sequences (KHS1, KHS27, KHS29). Grain size composition of lacustrine sediments from three cores at different sites and water depth in combination with lake carbonates, the occurrence/absence of ostracods and elevated paleo-shorelines reveal interconnected processes of sediment flux in response to water balance variations and climate change.

Distinguishing between wind-blown sediments and fluvial transport of suspended load is a challenge as grain size composition in lake deposits derived from both processes commonly overlap and merge into an integrated signal. Sediment type (grain size composition) of aeolian sediments depends on transport distance, transport height and wind velocity (Vandenberghe, 2013). Settled aeolian sediment in lacustrine systems thus can be similar to

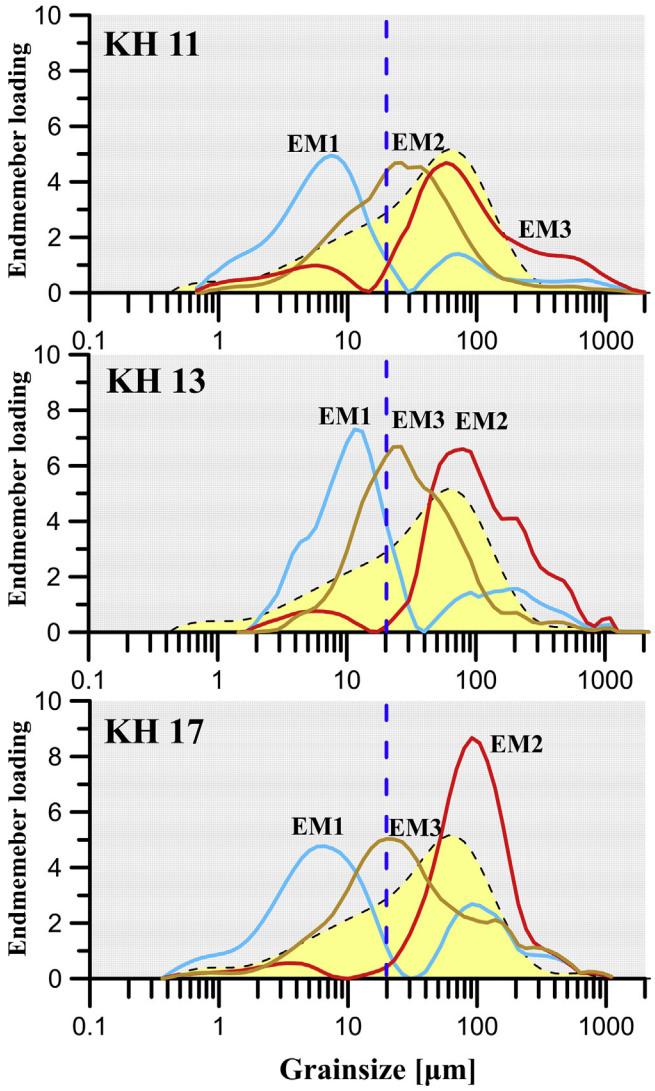

Fig. 8. Grain size endmember loadings of sediments from cores KH11, 13 and 17, underlain by the mean distribution curve of loess deposits in the Kuhai catchment (shaded in yellow). (For interpretation of the references to color in this figure legend, the reader is referred to the Web version of this article.)

suspended load components under low-energy fluvial transport but may display higher proportions of sand fractions and clay content with generally poorer sorting and decreased skewness (Vandenberghe, 2013 and references therein), depending on the distance between the sampling site and the inflowing water.

According to our grain size distribution curves derived from the cores KH11, 13 and 17 (Fig. 7) and respective unmixing by endmember analyses (Fig. 8) in comparison to the mean grain size distribution of loess deposits in the catchment, we distinguished sediment proportions in the sand fraction (>63 μm) that are assigned to fluvial transport including reworked and eroded aeolian sand under a closer distance between inflow and deposition site. Aeolian sand derived from exceptional storm events melting-out of ice-trapped sand fractions may have occasionally contributed to the overall sand budget. Some of the laminated sediment layers in a sediment core from the Lake Kuhai were assigned to pure aeolian deposits by Mischke et al. (2010).

Fine-clastic sediments below 20 μm were attributed to the main suspended load component (Fig. 9B and C) in accordance with the main modal values of EM1 and EM3 (EM2 in KH11) marking a boundary between coarser and finer fractions. Detrital flux derived from XRF data in the Kuhai records (Hu et al., 2018) widely correspond with suspended load data. Taking the mean percentages of the fine component (<20 μm) in loess and aeolian sand from the catchment into account (8.3–46%, Table S3), we presume that fluvially derived suspended load was always the major contributor through time. Much less proportions of dust input with comparable grain size derived from storm events were reported from Lake Sugan (Chen et al., 2013). In the Qinghai Lake region, An et al. (2012) used the 25 μm grain size value for the division between suspended load and westerly-derived aeolian dust as a base for the establishment of a so-called westerly index. Their results however, lack discussion in respect to catchment influences and the integration of suspended load with dust particles trapped in lake water.

5.1. Catchment-lake interactions

5.1.1. Aeolian and hydro-dynamic processes during the early and Mid-Holocene

Aeolian deposits are widespread within the Kuhai catchment. Notably, dune fields in the north-eastern catchment are associated with the episodically active drainage systems. These relatively small dune bodies of maximum 4 m individual height are semi-fixed by vegetation, except on their lake-ward sides (west to north-west direction) which indicate reactivation of sand transport. Although most of the investigated sections were located within the eastern catchment, aeolian sediments were also found in the western part, especially along the hillslopes facing towards the lake and on the larger island located in the southern part of the lake.

Aeolian deposits in sections outside the dune field mainly consisted of fine to medium sand (modes at 180–300 μm, mean: 200 μm), deposited at different times. Dune sands at the neighbouring Donggi Cona Lake basin provided similar grain size ranges (~210 μm, Stauch et al., 2012). Apparently, the source area for sand transportation was restricted to the catchment itself, namely along the drainages crossing the dune field. Other source areas were located along the shoreline and the sparsely vegetated alluvial fans in the north-western and south-western sub-catchments. According to the prevailing wind directions (mainly N, NW and W) in Kuhai lake area, erodible material was transported eastward resulting in higher accumulations on the eastern side of the lake and/or on the wind-shadow side of the hills along the western lake margin. These spatial distribution patterns were also observed in many other lake basins on the north-eastern Tibetan Plateau, such as Qinghai Lake, Donggi Cona and Hala Lake (Lu et al., 2011; Stauch et al., 2012; Wünnemann et al., 2012), for example. Their location mainly at the eastern sides of the basins indicate major influence by the mid-latitude westerlies (MLW) in combination with dry-cold winds from the Asian winter monsoon (Domroes and Peng, 1988) during phases of enhanced aeolian transport and deposition. Commonly, stronger winds occur in this larger region during early spring (Derbyshire et al., 1998; Han et al., 2008; Mao et al., 2011) as a result of the breakdown of the Siberian-Mongolian anticyclone and the northward shift of the westerly axis (Roe, 2009; Schiemann et al., 2009; Nagashima et al., 2013).

Interestingly, thick aeolian deposits, found on the southern island of Lake Kuhai, sands at the leeward side, were dated to between 11 and 9 ka and point to accumulation during the Early Holocene (KHS26 Fig. 4). Successions of sandy loess and loess deposits more uphill and on the north-eastern slope were younger and date to between 8 and 7 ka. These deposits were probably reworked by succeeding slope processes. Such old aeolian sands were not found at any other site in the Kuhai catchment and may point to wide-spread erosion of aeolian deposits in the eastern sub-catchments and/or re-mobilisation of sands during succeeding

periods (Qiang et al., 2014; Bailey and Thomas, 2014; Lu et al., 2015; Stauch, 2015, 2016).

Lake sediments in the deepest part of Lake Kuhai however, only partly resemble contemporaneous deposition of aeolian sand into an open water body. Instead we assume that erosion of aeolian material deposited in the eastern sub-catchments was mainly removed by fluvial processes as also discussed for the lack of Pleistocene aeolian deposits in the western Qaidam Basin (Yu et al., 2015). It remains an open question how these aeolian sands could reach the island across an open water body. Yan et al. (2017) found that the lack of aeolian sand in Daotanghe Pond close to Qinghai Lake was likely the result of a frozen water body, preventing aeolian sands from deposition in the pond during a period of the Little Ice Age (LIA). A similar situation may have occurred in Lake Kuhai, enabling the transport of sand across the closed ice cover from the western shore region to the rocky island during the frozen status. A lowered lake level at that time would have shortened the distance between the shore (exposed lake deposits) and the island.

The timing of eolian dynamics and deposition in the Kuhai catchment corresponds to OSL-dated sites in the Qinghai region, Gonghe, Zoige, and Donggi Cona Basins (Fig. 9A) which all indicate contemporaneous accumulation of aeolian sands and loess during the Late Glacial and Early Holocene periods (Yu and Lai, 2012; Stauch et al., 2012, 2014; Lu et al., 2015; Stauch, 2015; Qiang et al., 2016; Hu et al., 2018). These sand accumulations indicate the onset of their fixation due to wetter climate conditions (Stauch, 2018).

Frequent fluctuations in grain size between finer and coarser fractions (fluvial/aeolian) in core KH17 of Lake Kuhai during the Late Glacial (Younger Dryas) and Early Holocene periods (Fig. 9B and C), indicate alternating and probably unstable hydro-climatic conditions for transportation processes and lake fluctuations. As sediments in the core for this time period are similar to aeolian sand although slightly finer and alternating with fine-clastic suspended load (EMs in Fig. 8), we assume that phases of enhanced river inflow close to the core site was the major transportation medium. This indicates the onset of slightly wetter conditions than before, favouring lake level rise and the strong increase of carbonate precipitation in a warmer water body coupled with the increase of primary productivity (Fig. 9D) with the onset of the Holocene climate. Lake Kuhai changed from a pond-like setting with occasional occurrences of shallow water ostracods to a slightly increased lake stage with fluctuating lake levels. This assumption is different from the reported highest lake level of Lake Kuhai during the Early Holocene, exceeding the modern level by several tens of meter (Mischke et al., 2010). Presence of the shallow-water ostracod *L. inopinata* among others (*E. mareotica*, few *Ilyocypris* sp.) is a further indicator of a generally shallower lake (Fig. 9E).

Co-occurrence of aeolian deposits in catchment sections and adjacent regions during this period (Fig. 9A) confirms contemporaneous transportation processes. Beside the deposition of lacustrine sediments (slack water deposits) at the core sites a certain amount of wind-blown fine material trapped in ice with spatially different distribution also contributed to the overall sediment budget. Incorporation of dust particles and randomly distributed sand in frozen lake surfaces and ice cracks were reported by Opitz et al. (2012) and assigned to ice-rafted material in Hala Lake by Wang et al. (2015).

Enhanced fluvial activity compared to the previous period (Late Glacial: Younger Dryas), suggests the initiation of river incision into older alluvial fans and formed the higher terrace level (T1, Fig. 5) ca. 12–15 m above the modern river bed. The respective river system originates in the watershed area between the Kuhai and Yellow River catchments (eastern mountain chain). Due to the generally steep gradient of the river valley the incision rate might have been >1 mm/year. Two different processes may be responsible for terrace formation: i) a very low or temporarily non-existing lake, which would increase the flow gradient between the upper catchment and the lake basin, resulting in enhanced erosion by higher-energy flow. Another explanation could be that the driving factor for terrace formation was ii) tectonically induced uplift of the mountains which resulted in the same effect as mentioned before. The active left-lateral strike-slip Kunlun fault, tangential to Kuhai catchment in the south that induced the push-up structure of the Anyemaqen Mts (Van der Woerd et al., 2002; Fu et al., 2005) could be a likely mechanism to explain uplift of the eastern Kuhai catchment. However, it is most probable that both processes acted together and enabled strong river incision and thus terrace formation.

The lack of Mid-Holocene aeolian sand deposits between ca. 7.8 and 5 ka accords to few luminescence ages from sandy deposits in the adjacent regions for the same time interval. Only one section of sandy loess with an age of 6.8 ka was found in KHS25. Assuming that this is not only a random effect according to individual sampling strategies in the Kuhai catchment and other sites, we hypothesize that this period witnessed unfavourable conditions for aeolian mobility and deposition. Instead, more regular moister climate conditions, increased fluvial erosion accompanied by denser vegetation cover in source areas of potential deflation might be important reasons for the limitation of wind-blown sand transport and deposition (Fig. 9). The interaction of processes including morphology is outlined in the sketch across the Kuhai catchment for time intervals under warm/wet and colder/dryer conditions (Fig. 10).

Sediment composition in the lake center reveals highest amounts of fine-clastic sediment input, indicative of increased fluvial influx resulting in an overall positive water balance, notwithstanding a certain contribution of windblown sediments. The highest visible shoreline ca. 10 m above the present lake level (Mischke et al., 2010; Wünnemann et al., 2018) may have formed between ca. 7.5.and 5.5 cal ka BP, corresponding to the disappearance of ostracods and relatively constant carbonate precipitation (10–25%, Fig. 9D and E). Higher levels however, would have caused overflow to the Yellow-River system in the east. This phase of a higher lake level caused increased distance between the inflow regions and the core site, thus reducing the contribution of coarser grains to the lake center. Peaks of coarser grain size with modal values for sandy loess (65–75 μm, Fig. 9) at around 6.7 ka and between 6 and 5 ka however, might be caused by exceptionally high fluvial discharges or dust storm events during periods of unfrozen lake status. As corresponding aeolian sand was neither found in the Kuhai catchment nor in the other basins (Gonghe, Zoige, Qinghai) and only occasionally as sandy loess (KHS25 on the island) we tend to assign such grain size excursions to local short-term events without wide-spread preservation in the catchment.

Aeolian sediments in the loess fraction (including sandy loess) occurred at several places in the Kuhai catchment, even few meters above the modern lake level, of which three sections were luminescence dated. They indicate deposition between 9 and 5 ka and after 2 ka. (Fig. 9, Table S3). An altitudinal dependence of aeolian fractions as proposed for the Qilian Mt. region (Lehmkuhl, 1997; Nottebaum et al., 2014) in form of so-called “aeolian mantles” only partly applies to the Kuhai region. Sandy sediments occurred in the lower basin while loess/sandy loess and reworked loess was found in all altitudes above 4140 m a.s.l. Comparison with dated samples from the afore-mentioned basins, loess ages are distributed over the entire Holocene period which do not allow assigning depositional phases to certain climatic periods. This assumption is in accordance with findings by Stauch (2015) in the wider plateau region and indicates that loess transport and deposition occurred during all periods despite different climatic conditions as also

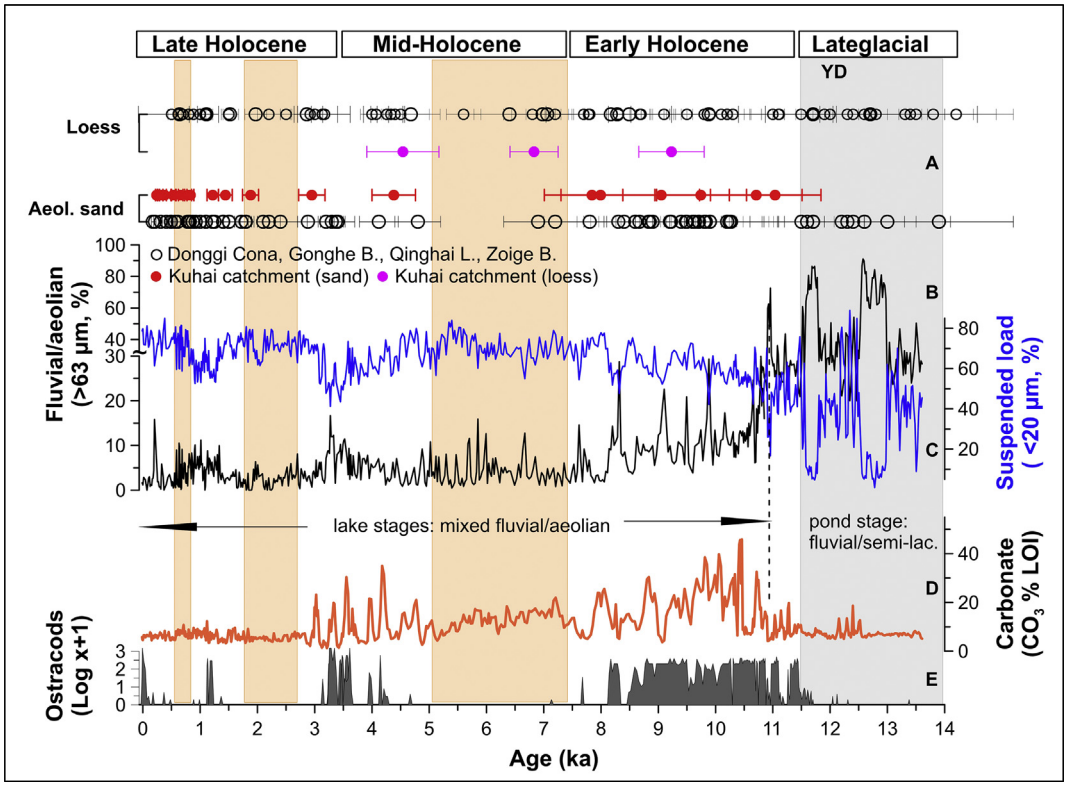

Fig. 9. (A) OSL ages from aeolian sediments (sand, loess) in sections of the Kuhai catchment in comparison with ages from adjacent regions; (B, C) grain size (fluvial/aeolian, >63 µm) and suspended load (<20 µm) records from core KH17, lake center; (D) carbonate (CO_3) content and (E) ostracod abundances. YD= Younger Dryas. Shaded areas (gray) mark the lateglacial period with negative water budget. Positive water balances with higher-than-present lake level refer to orange areas. (For interpretation of the references to color in this figure legend, the reader is referred to the Web version of this article.)

revealed by wetland deposits near Qinghai Lake for the last 1100 years (Yan et al., 2017).

5.1.2. Aeolian and fluvial interactions since the last 5 ka

The spatial distribution and timing of OSL-dated aeolian deposits in the larger region around the Kuhai catchment reveals few evidence for wind-blown sand deposits between ca. 5 ka and roughly 3 ka, although loess deposition indicates continuous aeolian transport (Fig. 9A). Only one dune body (bottom part) found in the Kuhai catchment points to deposition between 4.4 ka (K-feldspar age) and 3 ka (quartz-age). Sediment data from Lake Kuhai however, are evidence for a significant decline of slack water deposits (<20 µm, suspended load from river discharge) after ca 5.5 ka, culminating at ca. 3.5–3 cal ka BP. This trend is accompanied by increased sand input (Fig. 9C). According to discussed interactions between aeolian and fluvio-lacustrine processes during the Early Holocene and early Mid-Holocene periods, this pattern is likely associated with limited river discharge due to reduced effective moisture supply, expressed as relative increase of evaporation over precipitation (E/P ratio) and consequently a lowering of the lake level (e.g., Talbot, 1990; Fontes et al., 1996). The presence of ostracod species supports the argument for a rather shallow lake between 4.5 and 3.0 cal ka BP, evidenced by all cores (Fig. 11A and Fig. S12). This scenario however, would prefer the mobility of aeolian processes as outlined in Fig. 10B for low-lake level stages. The absence/reduction of wide-spread aeolian sand in onshore regions of Lake Kuhai and elsewhere however, can be attributed to the removal of sand during succeeding moister periods with increased fluvial activity and/or re-activation (reworking) of aeolian processes during dry phases of younger age. This phenomenon was also discussed by Stauch (2015) in respect to low data coverage for this time interval. On the other hand, re-activated aeolian sand in the Kubuqi sand sea of the northern Ordos Plateau during the Han and Tang Dynasties (206 BC-220 AD; 608–907 AD, respectively) might have been also initiated by human activity (Yang et al., 2016), which also could be an additional reason in Kuhai catchment.

Interestingly, this possible scenario cannot be inferred from the two other lake records (KH11, KH13, Fig. 11C and D) without considering the specific locations of the sites. The cores were retrieved from shallower water depth of which core KH11 was closer to the inflow regions of the episodically active drainage system. It is of importance that the river passes wide-spread wetlands before entering the lake. As a result, mainly fine-grained suspended load was transported to the core site while coarser grains were trapped by dense subaquatic vegetation in near-shore regions of the lake, similar to observed scenarios of today. Input of loess remained insignificant or involved in suspended load sediments (Fig. 7A). Considering a substantial decline in lake level during this time interval (Fig. 11A), both locations experienced extreme shallow water or extended wetland conditions with temporary dry phases. The core sites KH11 and KH13 were probably disconnected from the direct main inflow, resulting in reduced coarser fluvial sediment input while suspended load fractions could reach the site more frequently. Higher but inconsistent fluctuations in carbonate content compared to the core KH17 from the lake's center might be attributed to a local imprint by variable water coverage and/or changeable discharge behaviour of passing drainages. Wetland conditions would have protected the sites from wind-induced deflation and mobilisation processes. Parts of the sand fractions in KH11 and KH13 however, may be of aeolian origin. The reported differences between the sediment cores imply that

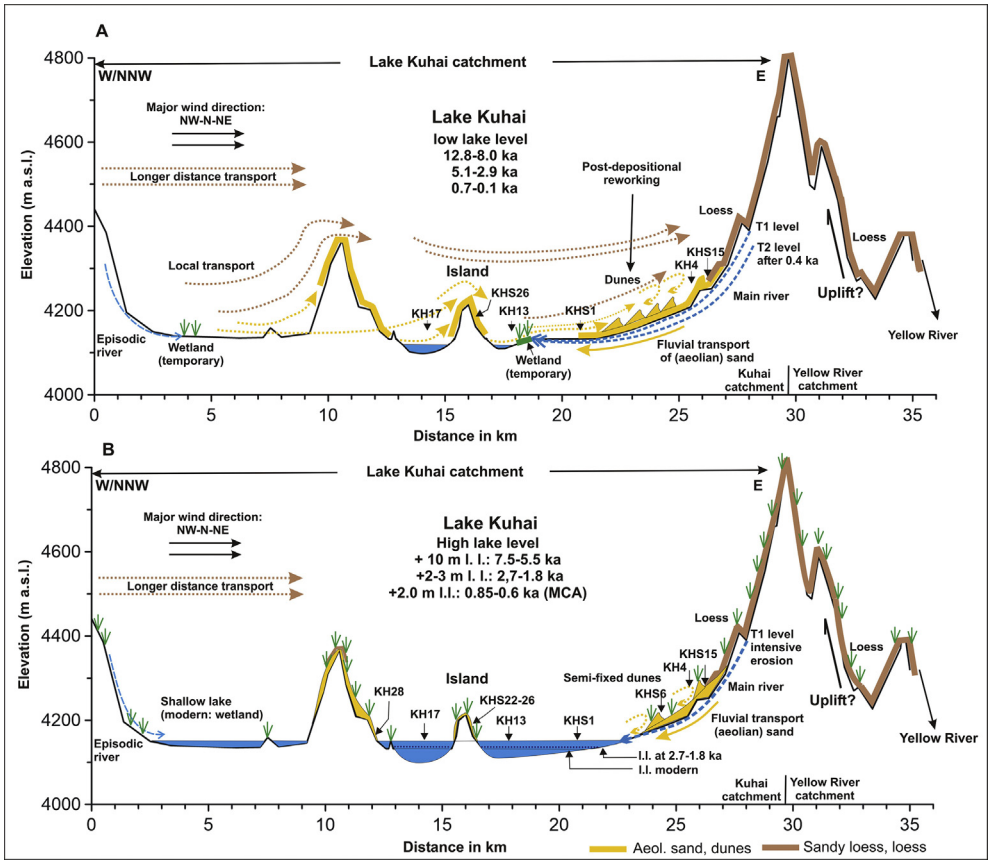

Fig. 10. Transect (sketch) across the Kuhai catchment from W/NNW to E. **(A)** Periods of higher lake level with reduced aeolian activity and higher river discharge/erosion (formation of terrace T1?) and **(B)** periods of low lake levels with stronger aeolian processes and reduced runoff. Dunes underwent several re-mobilisation phases after the early Holocene. River incision formed the terrace T2 after ca. 0.4 ka BP. Brown dotted lines with arrow indicate loess transport from local and longer distances; brown areas mark loess deposits. Yellow dotted lines with arrow indicate local sand transport; yellow areas depict aeolian sand sheets and dunes. Aeolian deposits, water depth and plant cover are unscaled. (For interpretation of the references to color in this figure legend, the reader is referred to the Web version of this article.)

environmental reconstruction and possible climate inferences strongly depend on the location of the selected sites as well as on a profound knowledge about processes in the attached sub-catchments. We speculate that without considering these interrelationships climate and environmental inferences may be incomplete of even misleading, if only one record is considered (see also Wünnemann et al., 2012).

A gap of luminescence ages between ca. 2.7 and 2.1 ka in the Kuhai catchment, Zoige Basin and Donggi Cona region is remarkable because the lake record KH17 (Fig. 11B) indicates reduced sand influx, generally high proportions of slack water and suspended load deposits (EM1 and EM3) and the lack of ostracod assemblages at three core sites (Fig. S12), all indicating higher-than present lake level. This relationship is less pronounced in the other two records (Fig. 11C and D) due to their closer position to the inflowing water and higher variability in the discharge behaviour (episodic) of the river near KH11 site. Radiocarbon-dated ostracod-bearing lacustrine sediments (near-shoreline facies) in sections KHS1 and KHS29 are in agreement with this inference.

The last 2 ka are well-documented in dated onshore sections and lake records. Aeolian sands and sandy loess indicate depositional phases in the Kuhai catchment between 1.9 and 0.3 ka (Fig. 11E), comparable with records from adjacent basins (Liu et al., 2011, 2015; Stauch, 2016; Qiang et al., 2016; Hu et al., 2018) suggesting that this period provided preferable conditions for sand transport, deposition and preservation. Intermediate fluctuations with probably enhanced dune formation are reported during the Dark Ages Cold Period (DACP) and LIA (Stauch, 2016). Increased sand influx between ca. 1.4 and 0.8 cal ka BP in cores KH13 and KH17, covering the DACP and parts of the following Medieval Climate Anomaly (MCA) matches luminescence-dated dune sand in Kuhai and Donggi Cona quite well. The inferred lower lake level may be the result of reduced discharge along the episodic rivers during the rainy summer season, as coarser sediments at site KH11 remained low in contrast to the other core sites where high sand influx dominated this period (Fig. 11A–D). The gravel layer in the river bank section KHS1 of the south-eastern perennial river at the same level with the modern lake falls into this time interval of the DACP.

An elevated lake level afterwards even 1–2 m above the present stage during the MCA is documented in the same section (KHS1) by a change from coarse gravels to ostracod-bearing sand-silt layers after 0.7 cal ka BP. This sequence points to flood-plain deposits which were deposited during overbank flow of a meandering river in close proximity of an elevated lake level (lowest flow gradient). Previously deposited aeolian sands may have been eroded during phases of river discharge and ingression of the lake into the valley (Fig. 6A). Ostracod communities (*E. mareotica* and *L. inopinata*) in general testify the deposition under a shallow aquatic environment with potential contribution of slightly flowing water as indicated by *L. inopinata* and *Ilyocypris* sp. (Meisch, 2000; Frenzel et al., 2010; Akita et al., 2016; Yan et al., 2017), perhaps with temporarily higher salinities (*E. mareotica,* Mischke, 2012; Yan and Wünnemann, 2014).

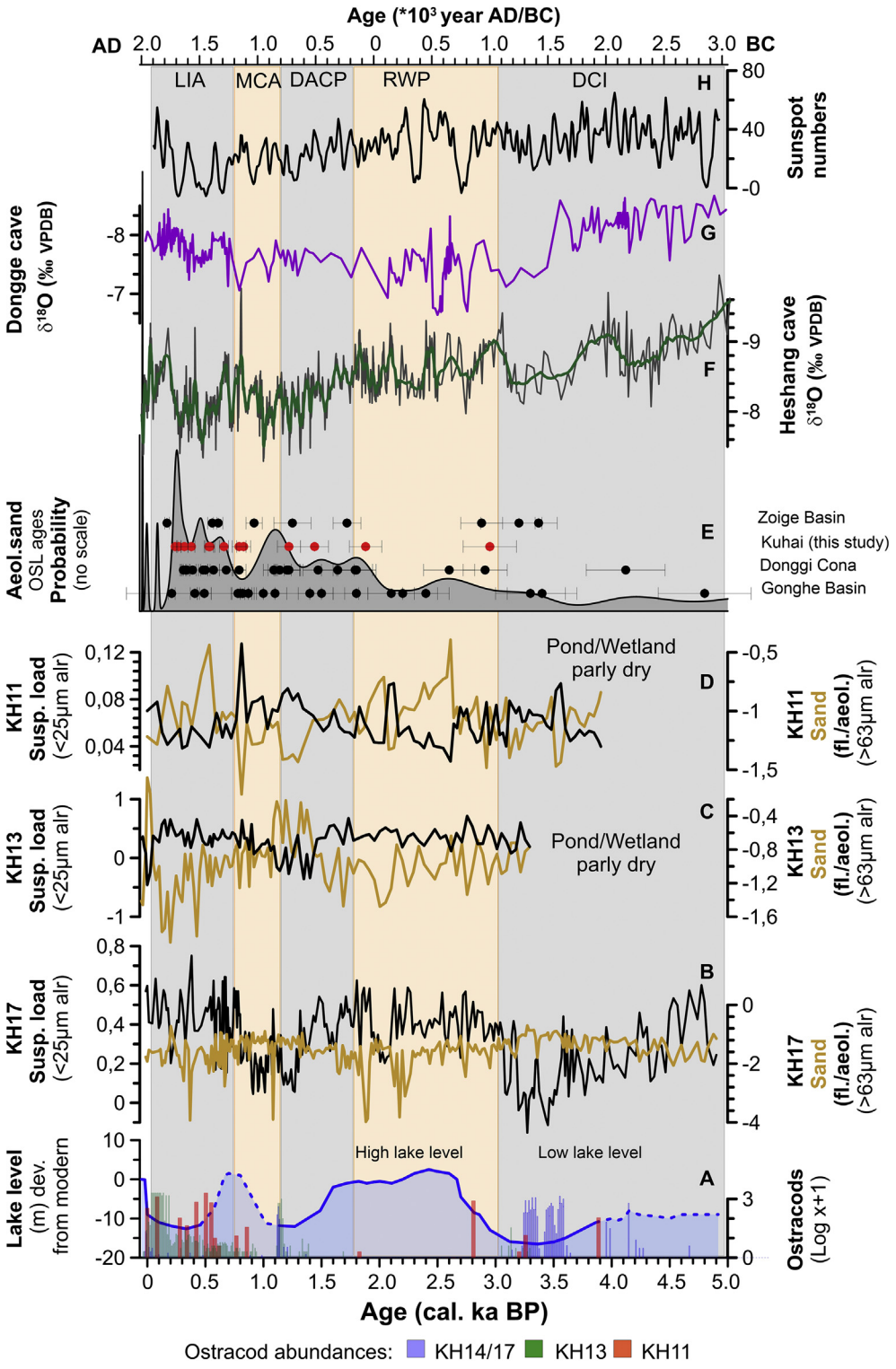

Fig. 11. Comparison of proxies from Lake Kuhai cores (B, C, D) for the last 5 ka with phases of aeolian sand deposition (E) in the Zoige Basin (Hu et al., 2018) Donggi Cona (Stauch et al., 2012, 2014) and Gonghe Basin (Stauch, 2016; Qiang et al., 2016) with background probability function of aeolian deposits for the last 5 ka (Stauch, 2016). Speleothem records (F) Heshang Cave: Hu et al., 2008, (G) Dongge Cave: Dykoski et al., 2006 and sunspot activity (H): Solanki et al., 2004. Lake level variations (A) were derived from ostracod occurrences, shoreline sections and fluvial discharge (suspended load input) with relative confidence (blue line) and estimation (dotted blue line). Shaded areas mark climatic units of colder/dryer conditions with lower lake levels (gray) and warmer/wetter conditions with higher lake levels (light orange). (For interpretation of the references to color in this figure legend, the reader is referred to the Web version of this article.)

The higher lake level during the MCA is indicated by aquatic plants (seagrass) in the shoreline section KHS29 (Fig. 6B) as well. They were washed ashore and deposited between shoreline gravels there. Also plant-rich semi-lacustrine sediments in section KHS27 ca. 1.3 m above the modern lake likely fall into the same period taking a certain RE of few hundred years for the dated plants/sediments into account (Table S2, Fig. 6 and Fig. S9). Comparable sections at Qinghai Lake pointing to a higher lake level were recently OSL-dated by Liu et al. (2015), based on near-shore sandy deposits or lacustrine sequences.

The period of the last ca. 700 years, covering the LIA, is recorded in several onshore sections by OSL-dated aeolian sand deposits, similar to the neighbouring Donggi Cona region (Stauch et al., 2012, 2014), indicative of higher aeolian mobility and preservation in dune bodies. Two paleosol layers in section KHS15 (Fig. 4B) however, indicate intermediate phases of soil formation at ca. 0.4–0.5 ka and 0.2 cal ka BP under slightly wetter conditions and perhaps reduced aeolian activity in the catchment. They developed contemporaneously with a 0.4 ka old plant-rich wetland layer found in terrace T2 (section KH9, Fig. 5). The silty soil layer in the upper part of section KHS1 (Fig. 6A) may point to the same age. Comparable environmental conditions were reported from the Daotanghe wetland near Qinghai Lake where variable sediment flux during the LIA (Yan et al., 2017), was interpreted as a non-uniform cold climate anomaly with intermediate phases of short-term positive water supply.

Sediments in the cores display an inconsistent pattern of strongly fluctuating suspended load and sand input. The general trend of a negative water balance coincides with high abundances of shallow water ostracods pointing to a lake level decline of >10 m in the lake center (KH17, Fig. 10A). The other two core sites experienced extremely shallow water or pond-like conditions, similar to those at 4-3 cal ka BP with locally different sediment flux. The strong incision into the terrace T2 along the south-eastern perennial river after ca. 0.4 ka is due to the lowered lake level and/or tectonic uplift. An erosion rate of approximately 2–3 mm/year for the 1.2 m high section KH9 can be assumed. A similar incision into former floodplain deposits could be observed in the neighbouring river bed from section KHS1. Both erosional processes correspond with increased river discharge during the last few centuries and subsequent lake level rise to its present height.

5.2. Climate inferences

Tectonic uplift of mountain ranges next to the Anyemaqen push-up structure may have modified erosion and sediment flux to Lake Kuhai, although geomorphological indicators for tectonic movements were not observed in the catchment. Therefore, major influencing factors that caused environmental changes were associated with hydro-climatic variations during the last ca 14 ka in response to the interplay between the ASM and MLW. Typical for lake basins in the semi-arid to arid regions of the TP, the interaction of aeolian, fluvial and fluvio-lacustrine processes strongly depended on water availability, commonly expressed as precipitation over evaporation (P/E) ratio (e.g., Talbot, 1990; Leng and Marshall, 2004; Wünnemann et al., 2018) and to a lesser extent on temperature. Modern available effective moisture in the Kuhai catchment is divided into summer rain during the monsoon season (July–Sept., ca. 54%) and snowfall/snowmelt (ca. 46%) in spring and late autumn according to climate data from the nearest weather station Maduo. Those data indicate seasonally different moistures sources either from the summer monsoon and local sources or the MLW that contribute to the overall water budget on the TP (Tian et al., 2007, 2008; Yao et al., 2013; Ren et al., 2013; Curio and Scherer, 2016; Yang and Yao, 2016). Recent modelling results based on deuterium excess in two ice cores from the north-western TP indicate that on average almost 50% of precipitation is contributed by local recycling during the past decades (An et al., 2017). This proportion however, underwent significant changes in the past (Wünnemann et al., 2018).

5.2.1. Late glacial-early Holocene climate

For the period of the Younger Dryas interval Lake Kuhai experienced a pond-like setting with variable input of sand by fluvial and aeolian processes. Low water availability was likely attributed to the lack of summer rainfall due to weak or absent summer monsoon effective moisture supply under colder climatic conditions mainly controlled by MLW climate (An et al., 2012; Liu et al., 2014).

Climate warming at the beginning of the Holocene coupled with the increase of effective moisture supply due to the recurrence of ASM impact (e.g., Wang et al., 2005; Dykoski et al., 2006; An, 2000, 2012; Liu et al., 2014) catchment-lake interactions generally accelerated. Speleothem records from the monsoon realm in China indicate strengthened summer monsoon influence with increased rainfall (Dykoski et al., 2006; Liu et al., 2014). Water supply and subsequent lake level rise of Lake Kuhai derived from high suspended load input was due to increased river discharge during the summer months. Lake level rise however, remained moderate. Aeolian sand transport was still a dominating factor in the catchment and contributed to the overall sediment input, resulting in the deposition of sand even on the southern island of the lake which was only possible under a lower lake level minimizing the distance between the source area (south-western shore) and the island.

Differently from the classical monsoon regions in China and the southern TP, we suppose that the north-eastern TP around Lake Kuhai remained less influenced by the ASM at that time as also reported for sites along the arid central Asia (ACA) domain (Chen et al., 2008). Frequent fluctuations in sediment input at Lake Kuhai during the Early Holocene (Fig. 9) however, points to rather unstable hydrologic conditions under a shallow aquatic system despite climate amelioration. This is supported by higher content of CO_3 and the occurrence of ostracods as well. Chen et al. (2008) argued that the influence of effective moisture supply by the East Asian Summer Monsoon (EASM) was still weak in comparison to classical monsoon regions in China. This assumption would support our results of hydro-climatic instability during the Early Holocene but conflicts with various other publications that indicate full monsoon climate during this period (e.g., Mischke et al., 2010; Zhang et al., 2011; An et al., 2012), summarized by Stauch (2015) with respect to aeolian activity. Those conflicting results might be attributed to regional differences in the distribution of effective moisture supply and related water vapour sources.

Rather unstable climatic conditions in the Kuhai region were likely linked with North Atlantic-derived climate anomalies that were associated with drift ice (Bond et al., 1997) and freshwater pulses (Alley et al., 1997; Fleitmann et al., 2003, 2008), both resulting in the slow-down of the meridional overturning circulation (AMOC, Bond et al., 2001). Those signals were transmitted by the MLW across the TP thus resulting in a dominant climatic factor in the wider region around Lake Kuhai. This general climate instability during the Early Holocene was inferred from various records worldwide (e.g., Alley et al., 1997; Bond et al., 1997; Von Grafenstein et al., 1999; Berner et al., 2010) and also in Chinese cave records (Wang et al., 2005; Liu et al., 2014), the Guliya ice core (Wang et al., 2002) and terrestrial records (Stauch, 2015) matching our inference for Lake Kuhai quite well. By contrast, stable oxygen isotope records from Qinghai Lake however, were interpreted in terms of intensified summer monsoon effective moisture supply during this period (Lister et al., 1991; Liu et al., 2007; An et al.,

2012), not in line with evidences from the Kuhai records. Chen et al. (2016) summarized some of the problems, which led to different interpretation. However, they also concluded a relatively dry Early Holocene.

5.2.2. Mid-Holocene climate

During the Mid-Holocene (ca. 7.5–5.5 ka) the lake and catchment experienced strongest fluvial activity, intensified erosion and further formation of terrace T1 accompanied by substantial lake level rise (positive water balance). Aeolian deposits in the catchment were eroded and formation of wind-blown features was limited or absent, indicated by the lack of luminescence-dated sediments in catchment sections and neighbouring regions. Apparently, these processes were associated with enhanced summer rainfall, resulting in the Mid-Holocene hydro-climatic optimum between roughly 7.5 and 5.1 cal ka BP. Furthermore, enhanced reworking of slope deposits was observed at several sites on the NE TP during this time (pers. comm. Stauch, Kaiser). This assumption supports the hypothesis that effective moisture supply by the EASM was more effective during the Mid-Holocene than during the previous period (Chen et al., 2008) as also inferred from lake records at Gonghai Lake (Chen et al., 2015; Rao et al., 2016) and from the loess plateau (Stauch, 2015), for example. This time lag in summer monsoon precipitation to insolation forcing (Zhang et al., 2017) might be attributed to the strong interplay between the ASM and the MLW as major controlling factors (An et al., 2012; Nagashima et al., 2013) in concert with local water vapour recycling processes inferred from modern scenarios (Ren et al., 2013; Yao et al., 2013; Curio and Scherer, 2016; An et al., 2017) at the marginal zone of summer monsoon influence of the north-eastern Tibetan Plateau in the past and present. However, it remains an open question whether amount-related summer monsoon rainfall in this region was responsible for an increased hydrological budget as inferred for Qinghai Lake north of Lake Kuhai (e.g., An et al., 2012).

5.2.3. Climate variations during the last 5 ka

The general decline of summer monsoon influence recorded in the Dongge and Heshang caves (Dykoski et al., 2006; Hu et al., 2008, Fig. 11F and G) after ca. 5 ka matches the decline of fine-clastic input into Lake Kuhai very well. Reduced discharge caused a substantial decline of the lake level (Fig. 11A) that favoured the re-occurrence of ostracod communities within a shallow lake environment and increased carbonate precipitation. This 2000-year long declining trend towards aridification and cooling in the Kuhai region corresponds well with weakened episodes of the ASM between ca. 4.5 and 3.0 ka, clearly traceable in the Dongge and Heshang caves with slight offsets in timing. Similar trends were also reported from Qinghai Lake (Hou et al., 2016), from Tso Kar and Tso Moriri in northern India (Demske et al., 2009; Wünnemann et al., 2010; Leipe et al., 2014) denoted to a dry-cold interlude (Dutt et al., 2018) and more precisely from the Cariaco Basin (Haug et al., 2001), likely caused by the southward shift of the intertropical convergence zone (ITCZ). The weakening of the ASM and stronger influence of the MLW on the north-eastern TP region explains the drastic decline in summer-related precipitation, severe lake level drops and enhanced aeolian activity during this period (Figs. 10A and 11A, E). The dramatic transformation of the Neolithic culture toward succeeding cultures in China (Liu and Feng, 2012), contemporaneous in timing with the collapse of the Indus Valley culture (Harappan civilization) in India (Staubwasser et al., 2003; Berkelhammer et al., 2012;) is perhaps associated with this climatic deterioration.

A reverse climatic trend with a significantly higher lake level, increased runoff, disappearance of ostracod communities and diminished preservation of aeolian deposits until ca 1.8 ka is recorded in the Kuhai records. This trend corresponds to enhanced but variable summer rainfall as shown in the afore-mentioned cave records. A general increasing trend of ASM influence as recorded in the Dongge cave (Dykoski et al., 2006), assigned to the so-called 2-ka-shift (Cheng et al., 2016) is not visible in the Heshang cave record and may indicate local to regional differences in the influence of summer monsoon effective moisture supply which also applies to the Kuhai region of generally limited ASM control. Fluctuations after ca. 1.8 ka correspond with cooling and desiccation periods during the DACP and LIA, interrupted by short-term positive water balance and related sediment fluxes during the MCA. These variations were also clearly documented in the aeolian sediment on the north-eastern Tibetan Plateau (Stauch, 2016). It was also suggested, that the influence of solar irradiation and related sunspot activity (Solanki et al., 2004; Steinhilber et al., 2012; An et al., 2012; Stauch, 2016) probably caused or amplified some of the recognized short-term shifts in summer monsoon-related effective moisture availability in favour of intensified MLW influence during decreased sunspot numbers (Fig. 11H). The close relationship between total solar irradiation and hydrological balance in the Daotanghe pond near Qinghai Lake was reported by Yan et al. (2017) and corresponds with intermediate periods of soil formation (wetter conditions) and reduced aeolian activity in the Kuhai catchment despite a general dominance of dry/cold climatic conditions during the LIA in both regions. Fluvial incision by about 2–3 mm yr^{-1} during the late stage of the LIA until the Present (terrace T2) is apparently caused by enhanced fluvial activity.

A recently published speleothem composite record from Xianglong cave by Tan et al. (2018) suggests opposite climate trends to well-known speleothem records in the wider region as well as the results from Lake Kuhai. In contrast to dry and colder climatic conditions during the DCI between ca. 4.5 and 3.0 ka, during the DACP and LIA in the Kuhai records the authors imply intensified monsoon precipitation for the same time intervals co-incident with recorded extreme flood events in the Hanjiang River region which could be doubtful. Moreover, reported extreme drought periods at 5 ka and 2.8 ka also do not correspond to our findings. These opposite interpretations of climate influence compared to neighbouring Heshang and Wanxiang cave sites (Hu et al., 2008; Zhang et al., 2008) however, are surprising and thus require more discussion.

6. Conclusion

Analyses of onshore sections and sediment cores from the Kuhai catchment and the lake basin located on the north-eastern TP are clear evidences for close links between on- and offshore processes related to aeolian and hydrodynamic mechanisms. Those interactions mainly responded to variations in the climate system during the Holocene. Reduced water availability accompanied by limited runoff and low lake levels corresponded with enhanced aeolian activity and dune formation. Such relationships were detectable in the sediment cores with locally different characteristics in relation to each distinct geomorphological settings including their positions and the distances to inflowing rivers. Increased water discharge resulting in positive water balance and higher-than-present lake levels of Lake Kuhai coincided with significantly reduced aeolian sand mobilisation and likely erosion of former sand deposits along drainage systems. Sand influx to the core sites remained low during these periods. Suspended load input smaller in grain size than typical loess served as an excellent recorder of river discharge intensity throughout the Holocene, although continuously mixed with aeolian components. Conversely, dated loess deposits in the Kuhai Basin and adjacent regions did not allow any differentiation between climatic stages as

they occurred at all periods under consideration. Water availability and related fluvial transport processes were linked to variable interactions between MLW and ASM. However, ASM imprint on the Kuhai region was likely not the only and/or dominant moisture source in the Kuhai region. Stronger MLW influence with potential teleconnection to North Atlantic climate anomalies are recorded in the catchment and lake deposits of the Kuhai basin and partly resemble changes in sunspot activity.

Acknowledgements

The research was funded by the 1000 Foreign Talents Programme granted by the Chinese Government to BW. Further funding was related to the distinguished professor and postdoc research funds from East China Normal University, Shanghai, Deutsche Forschungsgemeinschaft (DFG, WU270-10/3), NSFC grants 40971003, 41806105, post-doctoral grant 2018M630415 provided to DY by China Postdoctoral Science Foundation. HL thanks the Youth Innovation Promotion Association CAS (grant No. 2015251) for research fellowship. We thank professors K. L. Chen and G. L. Hou from Qinghai Normal University for their support in organising fieldwork. Thanks are also addressed to Dr. W.L. Xia for providing priority $^{210}Pb/^{137}Cs$ dating, Dr. L. Gao for support in luminescene dating, both from NIGLAS, as well as Mr. Y.B. Hu from Nanjing University and Mr. E. Runge from Freie Universität Berlin for grainsize analyses. We appreciate the help of German and Chinese students for support in field research.

Appendix A. Supplementary data

Supplementary data to this article can be found online at https://doi.org/10.1016/j.quascirev.2018.10.017.

References

Alley, R.B., Mayewski, P.A., Sowers, T., Stuiver, M., Taylor, K.C., Clark, P.U., 1997. Holocene climatic instability: a prominent, widespread event 8200 yr ago. Geology 25, 483–486.

Akita, L., Frenzel, P., Wang, J.B., Börner, N., Peng, P., 2016. Spatial distribution and ecology of the Recent Ostracoda from Tangra Yumco and adjacent waters on the southern Tibetan Plateau: a key to palaeoenvironmental reconstruction. Limnologica-Ecol. Manag. Inland Waters 59, 21–43.

An, Z.S., 2000. The history and variability of the East Asian paleomonsoon climate. Quat. Sci. Rev. 19 (1–5), 171–187.

An, Z., Colman, S., Zhou, W., Li, X., Brown, E., Timothy Jull, A., Cai, Y., Huang, Y., Lu, X., Chang, H., Song, Y., Xu, H., Liu, W., Jin, Z., Liu, X., Cheng, P., Liu, Y., Ai, L., Li, X., Liu, X., Yan, L., Shi, Z., Wang, X., Wu, F., Qiang, X., Dong, Z., Lu, F., Xu, X., 2012. Interplay between the Westerlies and Asian mo nsoon recorded in Lake Qinghai sediments since 32 ka. Sci. Rep. 2 (8), 619.

An, W., Hou, S., Zhang, Q., Zhang, W., Wu, S., Xu, H., Pang, H., Wang, Y., Liu, Y., 2017. Enhanced recent local moisture recycling on the northwestern Tibetan Plateau deduced from ice core deuterium excess. J. Geo. Res., Atmospheres 122, 12541–12556.

Bailey, R.M., Thomas, D.S.G., 2014. A quantitative approach to understanding dated dune stratigraphies. Earth Surf. Process. Landforms 39, 614–631.

Berkelhammer, M., Sinha, A., Stott, L., Cheng, H., Pausata, F.S.R., Yoshimura, K., 2012. An abrupt shift in the Indian monsoon 4000 years ago. In: Climates, Landscapes, and Civilizations (AGU Geophysical Monograph Series), pp. 75–87.

Berner, K.S., Koc, N., Godtliebsen, F., 2010. High frequency climate variability of the Norwegian Atlantic Current during the early Holocene period and a possible connection to the Gleissberg cycle. Holocene 20, 245–255.

Blaauw, M., Christen, J.A., 2011. Flexible paleoclimate age-depth models using an autoregressive gamma process. Bayesian Anal. 6, 457–474.

Bond, G., Showers, W., Cheseby, M., Lotti, R., Almasi, P., deMenocal, P., Priore, P., Cullen, H., Hajdas, I., Bonani, G., 1997. A pervasive millennial-scale cycle in North Atlantic Holocene and glacial climates. Science 278, 1257–1266.

Bond, G., Kromer, B., Beer, J., Muscheler, R., Evans, M.N., Showers, W., Hoffmann, S., Lotti-Bond, R., Hajdas, I., Bonani, G., 2001. Persistent solar influence on North Atlantic climate during the holocene. Science 294, 2130–2136.

Boos, W.R., Kuang, Z., 2010. Dominant control of the South Asian monsoon by orographic insulation versus plateau heating. Nature 463, 218–222.

Chen, F.H., Yu, Z.C., Yang, M.L., Ito, E., Wang, S.M., Madsen, D.B., Huang, X.Z., Zhao, Y., Sato, T., Birks, H.J.B., Boomer, I., Chen, J.H., An, C.B., Wünnermann, B., 2008. Holocene moisture evolution in arid central Asia and its out-of-phase relationship with monsoon history. Quat. Sci. Rev. 27, 351–364.

Chen, F.H., Qiang, M.R., Zhou, A.F., Xiao, S., Chen, J.H., Sun, D.H., 2013. A 2000- year dust storm record from Lake Sugan in the dust source area of arid China. J. Geophys. Res.: Atmosphere 118, 2149–2160.

Chen, F.H., Xu, Q.H., Chen, J.H., Birks, H.J.B., Liu, J.B., Zhang, S.R., Jin, L.Y., An, C.B., Telford, R.J., Cao, X.Y., Wang, Z.L., Zahng, X.J., Selvaraj, K., Lu, H.Y., Li, Y.C., Zheng, Z., Wang, H.P., Zhou, A.F., Dong, G.H., Zhang, J.W., Huang, X.Z., Bloemendal, J., Rao, Z.G., 2015. East Asian summer monsoon precipitation variability since the last deglaciation. Sci. Rep. 5, 11186. https://doi.org/10.1038/srep11186.

Chen, F., Wu, D., Chen, J., Zhou, A., Yu, J., Shen, J., Wang, S., Huang, X., 2016. Holocene moisture and East Asian summer monsoon evolution in the northeastern Tibetan Plateau recorded by Lake Qinghai and its environs: a review of conflicting proxies. Quat. Sci. Rev. 154, 111–129.

Cheng, H., Edwards, R.L., Sinha, A., Spötl, C., Yi, L., Chen, S., Kelly, M., Kathayat, G., Wang, X., Li, X., Kong, X., Wang, Y., Ning, Y., Zhang, H., 2016. The Asian monsoon over the past 640,000 years and ice age terminations. Nature 534, 640–646.

Colman, S.M., Yu, S.-Y., An, Z.S., Shen, J., Henderson, A.C.G., 2007. Late Cenozoic climate changes in China's western interior: a review of research on Lake Qinghai and comparison with other records. Quat. Sci. Rev. 26, 2281–2300.

Curio, J., Scherer, D., 2016. Seasonality and spatial variability of dynamic precipitation controls on the Tibetan Plateau. Earth Sys. Dyn. 7, 767–782.

Demske, D., Tarasov, P.E., Wünnemann, B., Riedel, F., 2009. Late glacial and Holocene vegetation, Indian monsoon and westerlies circulation in the Trans-Himalaya recordedin the lacustrine pollen sequence from Tso kar, Ladakh, NW India. Palaeogeogr. Palaeoclimatol. Palaeoecol. 279, 172–185.

Derbyshire, E., Meng, X., Kemp, R.A., 1998. Provenance, transport and characteristics of modern aeolian dust in western Gansu Province, China, and interpretation of the Quaternary loess record. J. Arid Environ. 39, 497–516.

Dietze, E., Diekmann, B., Wünnemann, B., Aichner, B., Hartmann, K., Herzschuh, U., IJmker, J., Jin, H., Kopsch, C., Lehmkuhl, F., Li, S., Mischke, S., Niessen, F., Opitz, S., Stauch, G., 2012. An end-member algorithm for deciphering modern detrital pro- cesses from lake sediments of Lake Donggi Cona, NE Tibetan Plateau, China. Sediment. Geol. 243–244, 169–180.

Dietze, E., Wünnemann, B., Hartmann, K., Diekmann, B., Jin, H., Stauch, G., Yang, S., Lehmkuhl, F., 2013. Early to mid-Holocene lake high-stand sediments at Lake Donggi Cona, northeastern Tibetan Plateau, China. Quat. Res. 79 (3), 325–336.

Domroes, M., Peng, G., 1988. The Climate of China. Springer, Berlin.

Dutt, S., Gupta, A.K., Wünnemann, B., Yan, D., 2018. A long arid interlude in the Indian summer monsoon during ~4,350 to 3,450 cal. yr BP contemporaneous to displacement of the Indus valley civilization. Quat. Int. 482, 83–92.

Dykoski, C.A., Edwards, R.L., Cheng, H., Yuan, D.X., Cai, Y.J., Zhang, M.L., Lin, Y.S., Qing, J.M., An, Z.S., Revenaugh, J., 2006. A high-resolution, absolute-dated Holocene and deglacial Asian monsoon record from Dongge Cave, China. Earth Planet Sci. Lett. 233, 71–86.

Fleitmann, D., Burns, S.J., Mudelsee, M., Neff, U., Kramers, J., Mangini, A., Matter, A., 2003. Holocene forcing of the Indian monsoon recorded in a stalagmite from Southern Oman. Science 300, 1737–1739.

Fleitmann, D., Mudelsee, M., Burns, S.J., Bradley, R.S., Kramers, J., Matter, A., 2008. Evidence for a widespread climatic anomaly at around 9.2 ka before present. Paleoceanography 23, PA1102. https://doi.org/10.1029/2007PA001519.

Frenzel, P., Wrozyna, C., Xie, M.P., Zhu, L.P., Schwalb, A., 2010. Palaeo-water depth estimation for a 600-year record from Nam Co (Tibet) using an ostracod-based transfer function. Quat. Int. 218, 157–165.

Folk, R.L., Ward, W.C., 1957. Brazos river bar: a study in the significance of grain size parameters. J. Sediment. Petrol. 27, 3–26.

Fontes, J.-C., Gasse, F., Gibert, E., 1996. Holocene environmental changes in Lake Bangong basin (Western Tibet). Part-1: chronology and stable isotopes of carbonates of a Holocene lacustrine core. Palaeogeogr. Palaeoclimatol. Palaeoecol. 120, 25–47.

Fu, B., Awata, Y., Du, J., He, W., 2005. Late Quaternary systematic stream offsets caused by repeated large seismic events along the Kunlun fault, northern Tibet. Geomorphology 71, 278–292.

Griffiths, H.I., Holmes, J.A., 2000. Non-marine Ostracods and Quaternary Palaeoenvironments. Quaternary Research Association, London.

Han, Y., Fang, X., Kang, S., Wang, H., Kang, F., 2008. Shifts of dust source regions over central Asia and the Tibetan Plateau econnections with the Arctic oscillation and the westerly jet. Atmos. Environ. 42, 2358–2368.

Haug, G.H., Hughen, K.A., Sigman, M., Peterson, L.C., Rohl, U., 2001. Southward migration of the intertropical convergence zone through the holocene. Science 293, 1304–1308.

Heiri, O., Lotter, A.F., Lemcke, G., 2001. Loss on ignition as a method for estimating organic and carbonate content in sediments: reproducibility and comparability of results. J. Paleolimnol. 25, 101–110.

Henderson, A.C.G., Holmes, J.A., Leng, M.J., 2010. Late Holocene isotope hydrology of Lake Qinghai, NE Tibetan Plateau: effective moisture variability and atmospheric circulation changes. Quat. Sci. Rev. 29, 2215–2223.

Holmes, J., Cook, E.R., Yang, B., 2009. Climate change over the past 2000 years in Western China. Quat. Int. 194, 91–107.

Hou, X. (Ed.), 2001. Vegetation Atlas of China. Science Press, Beijing.

Hou, J., Andrea, W.J.D., Liu, Z., 2012. The influence of ^{14}C reservoir age on interpretation of paleolimnological records from the Tibetan Plateau. Quat. Sci. Rev. 48, 67–79.

Hou, J., Huang, Y., Zhao, J., Liu, Z., Colman, S., An, Z., 2016. Large Holocene summer temperature oscillations and impact on the peopling of the northeastern

Tibetan Plateau. Geophys. Res. Lett. 43 (3), 1–8.
Hou, J., D'Andrea, W.J., Wang, M., He, Y., Liang, J., 2017. Influence of the Indian monsoon and the subtropical jet on climate change on the Tibetan Plateau since the late Pleistocene. Quat. Sci. Rev. 163, 84–94.
Hu, C.Y., Henderson, G.M., Huang, J.H., Xie, S.C., Sun, Y., Johson, k.R., 2008. Quantification of Holocene Asian monsoon rainfall from spatially separated cave records. Earth Planet Sci. Lett. 226, 221–232.
Hu, G., Yu, L., Dong, Z., Lu, J., Li, J., Wang, Y., Lai, Z., 2018a. Holocene aeolian activity in the Zoige Basin, northeastern Tibetan plateau, China. Catena 160, 321–328.
Hu, Y., Wünnemann, B., Zhang, Y., Yan, D., 2018b. Geochemistry record and its environmental implications during the past 14 ka in Kuhai Lake, NE Tibetan Plateau. Sedimentol. Sin. https://doi.org/10.14027/j.issn.1000-0550.2018.122 (in press).
IJmker, J., Stauch, G., Hartmann, K., Diekmann, B., Dietze, E., Opitz, S., Wünnemann, B., Lehmkuhl, F., 2012. Environmental conditions in the Donggi Cona lake catchment, NE Tibetan Plateau, based on factor analysis of geochemical data. J. Asian Earth Sci. 44, 176–188.
Kürschner, H., Herzschuh, U., Wagner, D., 2005. Phytosociological studies in the north-eastern Tibetan Plateau (NW China)—a first contribution to the subalpine scrub and alpine meadow vegetation. Botanische Jahrbücher der Systematik 126, 273–315.
Lehmkuhl, F., 1997. The spatial distribution of loess and loess-like sediments in the mountain areas of Central and High Asia. Z. Geomorph. N.F. Suppl. Bd. 111, 97–116.
Leipe, C., Demske, D., Tarasov, P.E., Wünnemann, B., Riedel, F., HIMPAC Project memers, 2014. A Holocene pollen record from the northwestern Himalayan lake Tso Moriri: implications for palaeoclimatic and archaeological research. Quat. Int. 348, 93–112.
Leng, M., Marshall, J., 2004. Palaeoclimate interpretation of stable isotope data from lake sediment archives. Quat. Sci. Rev. 23, 811–831.
Ling, X., 1999. Potential evaporation. In: Sun, H. (Ed.), The National Physical Atlas of China. China Cartographic Publishing House, Beijing, p. 88.
Lister, G.S., Kelts, K., Chen, K.Z., Yu, J.Q., Niessen, F., 1991. Lake Qinghai, China: closed-basin lake levels and the oxygen isotope record for ostracoda since the latest Pleistocene. Palaeogeogr. Palaeoclimatol. Palaeoecol. 84, 141–162.
Liu, X.Q., Shen, J., Wang, S.M., Wang, Y.B., Liu, W.G., 2007. Southwest monsoon changes indicated by oxygen isotope of ostracode shells from sediments in Qinghai Lake since the Late Glacial. Chin. Sci. Bull. 52, 539–544.
Liu, X., Lai, Z., Madsen, D., Yu, L., Liu, K., Zhang, J., 2011. Lake level variations of Qinghai Lake in northeastern Qinghai–Tibetan Plateau since 3.7 ka based on OSL dating. Quat. Int. 236, 57–64.
Liu, F.G., Feng, Z.D., 2012. A dramatic climatic transition at similar to 4000 cal. yr BP and its cultural responses in Chinese cultural domains. Holocene 22, 1181–1197.
Liu, Z., Wen, X., Brady, E.C., Otto-Bliesner, B., Yu, G., Lu, H., Cheng, H., Wang, Y., Zheng, W., Ding, Yihui, Edwards, R.L., Cheng, J., Liu, W., Yang, H., 2014. Chinese cave records and the east Asia summer monsoon. Quat. Sci. Rev. 83, 115–128.
Liu, J., Chen, J., Zhang, X., Li, Y., Rao, Z., Chen, F., 2015a. Holocene East Asian summer monsoon records in northern China and their inconsistency with Chinese stalagmite $d^{18}O$ records. Earth Sci. Rev. 148, 194–208.
Liu, X.J., Lai, Z.P., Madsen, D., Zeng, F.M., 2015b. Last deglacial and holocene lake level variations of lake Qinghai, northeastern Qinghai-Tibetan plateau. J. Quat. Sci. 30, 245–257.
Lockot, G., Ramisch, A., Wuennemann, B., Hartmann, K., Haberzettl, T., Chen, H., und, B.D., 2015. A process- and provenance-based attempt to unravel inconsistent radiocarbon chronologies in lake sediments – an example from Lake Heihai, North Tibetan Plateau (China). Radiocarbon 57, 1003–1019.
Long, H., Shen, J., Tsukamoto, S., Chen, J., Yang, L., Frenchen, M., 2014. Dry early Holocene revealed by sand dune accumulation chronology in Bayanbulak Basin (Xinjiang, NW China). Holocene 24, 612–624.
Lu, H.Y., Mason, J.A., Stevens, T., Zhou, Y.L., Yi, S.W., Miao, X.D., 2011. Response of surface processes to climatic change in the dunefields and Loess Plateau of North China during the late Quaternary. Earth Surf. Process. Landforms 36, 1590–1603.
Lu, R., Jia, F., Gao, S., Shang, Y., Li, J., Zhao, C., 2015. Holocene aeolian activity and climatic change in Qinghai Lake basin, northeastern Qinghai-Tibetan Plateau. Palaeogeogr. Palaeoclimatol. Palaeoecol. 430, 1–10.
Maussion, F., Scherer, D., Mölg, T., Collier, E., Curio, J., Finkelnburg, R., 2014. Precipitation seasonality and variability over the Tibetan plateau as resolved by the High Asia reanalysis. J. Clim. 27 (5), 1910–1927. https://doi.org/10.1175/JCLI-D-13-00282.1. ISSN 1520-0442. http://centaur.reading.ac.uk/69080/.
Mao, R., Ho, C.-H., Shao, Y., Gong, D.-Y., Kim, J., 2011. Influence of Arctic oscillation on dust activity over northeast Asia. Atmos. Environ. 45, 326–337.
Meisch, C., 2000. Freshwater Ostracoda of Western and Central Europe. Spektrum Akademischer Verlag, Heidelberg.
Mischke, S., Kramer, M., Zhang, C.J., Shang, H.M., Herzschuh, U., Erzinger, J., 2008. Reduced early Holocene moisture availability in the Bayan Har Mountains, northeastern Tibetan Plateau, inferred from a multi-proxy lake record. Palaeogeogr. Palaeoclimatol. Palaeoecol. 267, 59–76.
Mischke, S., Zhang, C., Börner, A., Herzschuh, U., 2010. Lateglacial and Holocene variation in aeolian sediment flux over the northeastern Tibetan Plateau recorded by laminated sediments of a saline meromictic lake. J. Quat. Sci. 25, 162–177.
Mischke, S., Zhang, C.J., 2010. Holocene cold events on the Tibetan plateau. Glob. Planet. Change 72, 155–163.
Mischke, S., 2012. Quaternary ostracods from the Tibetan Plateau and their significance for envi- ronmental and climate-change studies. Dev. Quat. Sci. 17, 263–279.
Mischke, S., Weynell, M., Zhang, C., Wiechert, U., 2013. Spatial variability of ^{14}C reservoir effects in Tibetan Plateau lakes. Quat. Int. 313–314, 147–155.
Morrill, C., Overpeck, J.T., Cole, J.E., Liu, K., Shen, C., Tang, L., 2006. Holocene variations in the Asian monsoon inferred from the geochemistry of lake sediments in central Tibet. Quat. Res. 65, 232–243.
Nagashima, K., Tada, R., Toyoda, S., 2013. Westerly jet-East Asian summer monsoon connection during the Holocene. G-cubed 14 (12), 5041–5053.
Nottebaum, V., Lehmkuhl, F., Stauch, G., Hartmann, K., Wünnemann, B., Schimpf, S., Lu, H., 2014. Regional grain size variations in aeolian sediments along the transition between Tibetan highlands and north-western Chinese deserts – the influence of geomorphological settings on aeolian transport pathways. Earth Surf. Process. Landforms. https://doi.org/10.1002/esp.3590.
Opitz, S., Wünnemann, B., Aichner, B., Dietze, E., Hartmann, K., Herzschuh, U., IJmker, J., Lehmkuhl, F., Li, S., Mischke, S., Plotzki, A., Stauch, G., Diekmann, B., 2012. Late glacial and Holocene development of Lake Donggi Cona, northeastern Tibetan Plateau, inferred from sedimentological analysis. Palaeogeogr. Palaeoecol. Palaeoclimatol. 337–338, 159–176.
Qiang, M.R., Liu, Y.Y., Jin, Y.X., Song, L., Huang, X.T., Chen, F.H., 2014. Holocene record of eolian activity from genggahai lake, northeastern Qinghai-Tibetan plateau, China. Geophys. Res. Lett. 41, 589–595.
Qiang, M., Jin, Y., Liu, X., Song, L., Li, H., Li, F., Chen, F., 2016. Late pleistocene and holocene aeolian sedimentation in Gonghe Basin, northeastern Qinghai-Tibetan Plateau: variability, processes, and climatic implications. Quat. Sci. Rev. 132, 57–73.
Qiang, M., Song, L., Jin, Y., Li, Y., Liu, L., Zhang, J., Zhao, Y., Chen, F., 2017. A 16-ka oxygen-isotope record from Genggahai Lake on the northeastern Qinghai-Tibetan Plateau: hydroclimatic evolution and changes in atmospheric circulation. Quat. Sci. Rev. 162, 72–87.
Ramisch, A., Lockot, G., Haberzettl, T., Hartmann, K., Kuhn, G., Lehmkuhl, F., Schimpf, S., Schulte, P., Stauch, G., Wang, R., Wünnemann, B., Yan, D., Zhang, Y., Diekmann, B., 2016. A persistent northern boundary of indian summer monsoon precipitation over central Asia during the holocene. Sci. Rep. 6, 25791.
Rao, Z., Jia, G., Li, Y., Chen, J., Xu, Q., Chen, F., 2016. Asynchronous evolution of the isotopic composition and amount of precipitation in north China during the Holocene revealed by a record of compound-specific carbon and hydrogen isotopes of long-chain *n*-alkanes from an alpine lake. Earth Planet Sci. Lett. 446, 68–76.
Reimer, J.P., Bard, E., Bayliss, A., Beck, J.W., Blackwell, P.G., Ramsey, C.B., Brown, D.M., Guil derson, T.P., Haflidason, H., Hajdas, I., Hatté, C., Heaton, T.J., Hogg, A.G., Hughen, K.A., Kai ser, K.F., Kromer, B., Manning, S.W., Reimer, R.W., Richards, D.A., Scott, E.M., Southon, J.R., Turney, C.S.M., Van Der Plicht, J., 2013. Intcal13 and Marine13 radio- carbon age calibration curves 0–50,000 Years cal bp. Radiocarbon 55, 1869–1887.
Ren, W., Yao, T., Yang, X., Joswiak, D.R., 2013. Implications of variations in $d^{18}O$ and dD in precipitation at Madoi in the eastern Tibetan Plateau. Quat. Int. 313, 56–61.
Roe, G., 2009. On the interpretation of Chinese loess as a paleoclimate indicator. Quat. Res. 71, 150–161.
Rother, H., Stauch, G., Loibl, D., Lehmkuhl, F., Freeman, S.P.H.T., 2017. Late Pleistocene glaciations at Lake Donggi Cona, eastern Kunlun Shan (NE Tibet): early maxima and a diminishing trend of glaciation during the last glacial cycle. Boreas 46, 503–524. https://doi.org/10.1111/bor.12227.
Schiemann, R., Lüthi, D., Schär, C., 2009. Seasonality and interannual variability of the westerly jet in the Tibetan Plateau region. J. Clim. 22 (11), 2940–2957.
Solanki, S.K., Usoskin, I.G., Kromer, B., Schüssler, M., Beer, J., 2004. An unusually active Sun during recent decades compared to the previous 11,000 years. Nature 431, 1084–1087.
Staubwasser, M., Sirocko, F., Grootes, P.M., Segl, M., 2003. Climate change at the 4.2 ka BP termination of the Indus valley civilization and Holocene south Asian monsoon variability. Geophys. Res. Lett. 30, 1425. https://doi.org/10.1029/2002GL016822.
Stauch, G., IJmker, J., Pötsch, S., Zhao, H., Hilgers, A., Diekmann, B., Dietze, E., Hartmann, K., Opitz, S., Wünnemann, B., Lehmkuhl, F., 2012. Aeolian sediments on the north-eastern Tibetan Plateau. Quat. Sci. Rev. 57, 71–84.
Stauch, G., Poetsch, S., Zhao, H., Lehmkuhl, F., 2014. Interaction of geomorphological processes on the north-eastern Tibetan Plateau during the holocene, an example from a sub-catchment of lake Donggi Cona. Geomorphology 210, 23–35.
Stauch, G., 2015. Geomorphological and palaeoclimate dynamics recorded by the formation of aeolian archives on the Tibetan Plateau. Earth Sci. Rev. 150, 393–408.
Stauch, G., 2016. Multi-decadal periods of enhanced aeolian activity on the north-eastern Tibet Plateau during the last 2ka. Quat. Sci. Rev. 149, 91–101.
Stauch, G., 2018. A conceptual model for the interpretation of Aeolian sediments from a semiarid high-mountain environment since the late glacial. Quat. Res. 1–18.
Steinhilber, F., Abreu, J.A., Beer, J., Brunner, I., Christl, M., Fischer, H., Heikkil€a, U., Kubik, P.W., Mann, M., McCracken, K.G., Miller, H., Miyahara, H., Oerter, H., Wilhelms, F., 2012. 9,400 years of cosmic radiation and solar activity from ice cores and tree rings. Proc. Natl. Acad. Sci. U. S. A 109, 5967–5971.
Talbot, M.R., 1990. A review of the palaeohydrological interpretation of carbon and oxygen isotopic ratios in primary lacustrine carbonates. Chem. Geol. 80, 261–279.

Tian, L., Yao, T., MacClune, K., White, J.W.C., Schilla, A., Vaughn, B., Vachon, R., Ichiyanagi, K., 2007. Stable isotopic variations in west China: a consideration of moisture sources. J. Geophys. Res. 112. D10112. https://doi.org/10.1029/2006JD007718.

Tian, L., Ma, L., Yu, W., Liu, Z., Yin, C., Zhao, Z., Tang, W., Wang, Y., 2008. Seasonal variations of stable isotope in precipitation and moisture transport at Yushu, eastern Tibetan Plateau. Sci. China (Series D) 51 (8), 1121–1128.

Tan, L., Cai, Y., Cheng, H., Edward, L.R., Gao, Y., Xua, H., Zhang, H., An, Z., 2018. Centennial-to decadal-scale monsoon precipitation variations in the upper Hanjiang River region, China over the past 6650 years. Earth Planet Sci. Lett. 482, 580–590.

Vandenberghe, J., 2013. Grainsize of fine-grained windblown sediment: a powerful proxy for process identification. Earth Sci. Rev. 121, 18–30.

Van der Woerd, J., Tapponnier, P., Ryerson, F.J., Meriaux, A.-S., Meyer, B., Gaudemer, Y., Finkel, R.C., Caffee, M.W., Guoguang, Z., Zhiqin, X., 2002. Uniform postglacial slip- rate along the central 600 km of the Kunlun Fault (Tibet), from 26Al, 10Be, and 14C dating of riser offsets, and climatic origin of the regional morphology. Geophys. J. Int. 148, 356–388.

Van der Meeren, T., Khand, Y., Martens, K., 2015. On recent species of Tonnacypris Diebel & Pietrzeniuk, 1975 (Crustacea, Ostracoda), with new species descriptions from Mongolia. Zootaxa 2009, 1–41.

Von Grafenstein, U., Erlenkeuser, H., Brauer, A., Jouzel, J., Johnsen, S.J., 1999. A mid-European decadal isotope-climate record from 15,500 to 5000 years BP. Science 284, 1654–1657.

Wang, N.L., Yao, T.D., Thompson, L.G., Henderson, K.A., Davis, M.E., 2002. Evidence for cold events in the early Holocene from the Guliya ice core, Tibetan Plateau, China. Chin. Sci. Bull. 47, 1422–1427.

Wang, Y.J., Cheng, H., Edwards, R.L., He, Y.Q., Kong, X.G., An, Z.S., Wu, J.Y., Kelly, M.J., Dykoski, C.A., Li, X.D., 2005. The Holocene Asian monsoon: links to solar changes and North Atlantic climate. Science 308, 854–857.

Wang, R., Zhang, Y.Z., Wünnemann, B., Biskaborn, B.K., Yin, H., Xia, F., Zhou, L.F., Diekmann, B., 2015. Linkages between quaternary climate change and sedimentary processes in Hala Lake, northern Tibetan plateau, China. J. Asian Earth Sci. 107, 140e150.

Weltje, G.J., 1997. End-member modeling of compositional data: numerical- statistical, algorithms for solving the explicit mixing problem. J. Math. Geol. 29, 503–549.

Wu, Y., Lücke, A., Jin, Z., Wang, S., Schleser, G.H., Battarbee, R.W., Weilan, X., 2006. Holocene climate development on the central Tibetan Plateau: a sedimentary record Cuoe Lake. Palaeogeogr. Palaeoclimatol. Palaeoecol. 234, 328–340.

Wu, Y., Li, S., Lücke, A., Wünnemann, B., Zhou, L., Reimer, P., Wang, S., 2009. Lacustrine radiocarbon reservoir ages in Co ngoin and zige tangco, central Tibetan plateau. Quat. Int. 212, 21–25.

Wünnemann, B., Demske, D., Tarasov, P., Kotlia, B.S., Reinhardt, C., Bloemendal, J., Diekmann, B., Hartmann, K., krois, J., Reidel, F., Arya, N., 2010. Hydrological evolution during the last 15 kyr in the Tso Kar lake basin (Ladakh, India), derived from geomorphological, sedimentological and palynological records. Quat. Sci. Rev. 29, 1138–1155.

Wünnemann, B., Wagner, J., Zhang, Y., Yan, D., Wang, R., Yan, S., Fang, X., Zhang, J., 2012. Implications of diverse sedimentary patterns in Hala Lake, Qinghai province, China for reconstructing late quaternary climate. J. Paleolimnol. 48, 725–749.

Wünnemann, B., Yan, D., Ci, R., 2015. Morphodynamics and lake level variations at Paiku Co, southern Tibetan Plateau, China. Geomorphology 246, 489–501.

Wünnemann, B., Yan, D., Andersen, N., Riedel, F., Zhang, Y., Sun, Q., Hoelzmann, P., 2018. A 14 ka high-resolution δ18O lake record reveals a paradigm shift for the process-based reconstruction of hydroclimate on the northern Tibetan Plateau,. Quat.Sci.Rev. 200, 65–84.

Yan, D., Wünnemann, B., 2014. Late quaternary water depth changes in Hala Lake, northeastern Tibetan plateau, derived from ostracod assemblages and sediment properties in multiple sediment records. Quat. Sci. Rev. 95, 95–114.

Yan, D., Wuennemann, B., Hu, Y., Frenzel, P., Zhang, Y., Chen, K., 2017. Wetland evolution in the Qinghai Lake area, China, in response to hydrodynamic and eolian processes during the past 1100 years. Quat. Sci. Rev. 162, 42–59.

Yan, D., 2017. Interplay between Lake and Catchment Processes in Kuhai Lake Basin, NE Tibetan Plateau, China during Late Holocene. Dissertation Dept. of Earth Science, Freie Universität Berlin.

Yang, X., Forman, F., Hu, F., Zhang, D., Liu, Z., Li, J., 2016. Initial insights into the age and origin of the Kubuqi sand sea of northern China. Geomorphology 259, 30–39.

Yang, X., Yao, T., 2016. Different sub-monsoon signals in stable oxygen isotope in daily precipitation to the northeast of the Tibetan Plateau. Tellus B 68, 27922.

Yao, T., Masson-Delmotte, V., Gao, J., Yu, W., Yang, X., Risi, C., Sturm, C., Werner, M., Zhao, H., He, Y., Ren, W., Tian, L., Shi, C., Hou, S., 2013. A review of climatic controls on d^{18}O in precipitation over the Tibetan plateau: observations and simulations. Rev. Geophys. 51, 525–548.

Yu, L., Lai, Z., 2012. OSL chronology and palaeoclimatic implications of aeolian sediments in the eastern Qaidam Basin of the northeastern Qinghai-Tibetan Plateau. Palaeogeogr. Palaeoclimatol. Palaeoecol. 337–338, 120–129.

Yu, L., Lai, Z., An, P., Pan, T., Chang, Q., 2015. Aeolian sediments evolution controlled by fluvial processes, climate change and human activities since LGM in the Qaidam Basin, QinghaieTibetan Plateau. Quat. Int. 372, 23–32.

Zhang, H.C., Ming, Q.Z., Lei, G.L., Zhang, W.X., Fan, H.F., Chang, F.Q., Wünnemann, B., Hartmann, K., 2006. Dilemma of dating on Lacustrine deposits in an hyperarid inland basin of NW China. Radiocarbon 48, 210–226.

Zhang, C.J., Mischke, S., 2009. A Lateglacial and Holocene lake record from the Nianbaoyeze Mountains and inferences of lake, glacier and climate evolution on the eastern Tibetan Plateau. Quat. Sci. Rev. 28, 1970–1983.

Zhang, P., Cheng, H., Edwards, R., Chen, F., Wang, Y., Yang, X., Liu, J., Tan, M., Wang, X., Liu, J., An, C., Dai, Z., Zhou, J., Zhang, D., Jia, J., Jin, L., Jonson, K., 2008. A test of climate, sun and culture relationships from an 1810-year Chinses Cave Record. Science 322, 940–942.

Zhang, J.W., Chen, F.H., Holmes, J.A., Li, H., Guo, X.Y., Wang, J.L., Li, S., Lü, Y.B., Zhao, Y., Qiang, M.R., 2011. Holocene monsoon climate documented by oxygen and carbon isotopes from lake sediments and peat bogs in China: a review and synthesis. Quat. Sci. Rev. 30, 1973–1987.

Zhang, X., Liya Jin, L., Chen, J., Lu, H., Chen, F., 2017. Lagged response of summer precipitation to insolation forcing on the northeastern Tibetan Plateau during the Holocene. Clim. Dynam. https://doi.org/10.1007/s00382-017-3784-9.